# Theory of ultrafast electron diffraction: The role of the electron bunch properties

A. M. Michalik, E. Ya. Sherman, and J. E. Sipe

Citation: Journal of Applied Physics **104**, 054905 (2008); doi: 10.1063/1.2973157
View online: https://doi.org/10.1063/1.2973157
View Table of Contents: http://aip.scitation.org/toc/jap/104/5
Published by the American Institute of Physics

# Theory of ultrafast electron diffraction: The role of the electron bunch properties

A. M. Michalik,[1] E. Ya. Sherman,[1,2] and J. E. Sipe[1]
[1]*Department of Physics and Institute for Optical Sciences, University of Toronto, 60 St. George Street, Toronto, Ontario M5S 1A7, Canada*
[2]*Department of Chemical Physics, University of the Basque Country UPV/EHU, 48080 Bilbao, Spain*

(Received 2 May 2008; accepted 20 June 2008; published online 5 September 2008)

We present a general formalism for scattering of electron bunches used in ultrafast electron diffraction experiments. To perform the scattering calculation, we associate the classical distribution function that describes the electron bunch just before scattering with the asymptotic-in Wigner distribution. Using single scattering and far-field approximations, we derive an expression for the diffracted signal and discuss the effects of the different bunch parameters on the measured diffracted flux. We identify the transverse and longitudinal coherence lengths and discuss the importance of these length scales in diffraction pattern formation. We present sample numerical calculations for scattering by nanosize particles based on our model and discuss the results in terms of bunch and scattering target parameters. © *2008 American Institute of Physics*. [DOI: 10.1063/1.2973157]

## I. INTRODUCTION

Ultrafast electron diffraction (UED) is an experimental technique used to study the evolution of atomic, molecular, and condensed matter systems on pico- and subpicosecond time scales. It has recently been applied to study phase transitions in metallic thin films,[1–5] molecular transformations and chemical reactions,[6–12] and surface dynamics[13–15] and stand-alone nanostructures.[16] An experimental run typically consists of three stages (Fig. 1). In the first stage, a cathode is subjected to a laser pulse of about 100 fs, and an electron bunch of about $10^4$ electrons is photoemitted and accelerated to energies of 30 keV or higher. In the second stage the bunch propagates to the target. In the third stage the bunch scatters from the target, and a diffraction pattern is observed. The somewhat artificial division of the experiment into these stages is useful because different theoretical techniques can be used in the analysis of each.

In a previous paper[17] we examined the electron dynamics in the second stage. During this stage space-charge effects are critically important. As the bunch propagates it expands due to Coulomb repulsion and the initial momentum spread, which results in a strong correlation between the position and the velocity of electrons in the bunch. The phase-space density in this stage, however, is low enough that the bunch can be treated by the techniques of classical mechanics. A classical phase-space distribution function can be introduced and its evolution can be calculated by employing either numerical simulations or approximate analytic approaches. In our paper[17] we explored the use of a simple analytic model to describe the electron dynamics, and found excellent agreement with many-body numerical simulations.

The third stage is the subject of this paper. Here, classical dynamics must be abandoned since we seek a description of the diffraction of the electrons by the target, which is manifestly a quantum mechanical effect. However, by the time the bunch arrives at the target it has been sufficiently dispersed that Coulomb effects between the electrons in the bunch are negligible, and only the interaction between the electrons and the target is important. Thus the scattering of the bunch essentially reduces to a single-particle scattering problem. Coulomb effects can also be neglected in the post-target region. In principle, strong focusing of the bunch could require the inclusion of Coulomb effects on bunch propagation after the target, but in practice such focusing would be well outside the normal range of UED experimental parameters. For simplicity, we omit any discussion of post-target focusing. Even though Coulomb effects are neglected during bunch scattering, a simple plane wave analysis is not sufficient because of the limited coherence of the bunch. We proceed with a general analysis that lets us characterize the dependence of the detected diffraction signal on the properties of the incident bunch at the target.

The general scattering formalism we present associates a Wigner distribution function with the incident electron bunch. It includes all three possible combinations of scattered and unscattered components of the bunch. These combinations result in a holographic signal that captures the interference between the unscattered part of the bunch and a diffraction signal. In typical UED experiments, the holographic signal is confined to very small angles in the forward direction and is thus not detected; we defer to a later publication a discussion of new experimental scenarios in which it might be accessible. Our focus here will be only on the diffraction signal.

We explore the far-field limit of the diffraction signal,

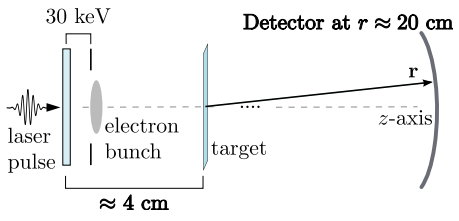


FIG. 1. (Color online) A simple sketch of the UED experiment.

 

where the electron wavelength is much smaller than the post-target distance, and identify how the bunch and target properties affect the observed signal. Simplifications of the diffraction expression are possible because of the conditions of typical UED experiments, where low coherence and small illumination angles lead to a set of inequalities that can be employed in an asymptotic analysis of the signal. We find that the width of the diffraction peak is set by the lateral coherence of the bunch, the transverse momentum spread, and the domain size if the target is crystalline. The relatively small spread in the electron wavelength of the bunch plays a negligible role in the pattern formation.

Since the diffraction pattern is not focused, in contrast to electron propagation in a transmission electron microscope, a Fraunhöfer-type analysis is found suitable only for small samples. For large targets, such as thin films, a Fresnel-type analysis taking into account the limited coherence of the electron bunch is required. In this case the diffraction pattern can include a complex convolution of the real- and reciprocal-space information of both the bunch and target properties. The far-field expression we derive is amenable to numerical simulations, and we present sample calculations that illustrate the effects of both the bunch parameters and target properties on the diffraction signal.

This paper is organized as follows. Section II introduces the single-particle Wigner function that represents the electron bunch, and the important distribution parameters that characterize it. In Sec. III we derive a general expression for the scattering electron flux which forms the diffraction pattern. In Sec. IV we proceed with the simplification of the diffraction expression in the far-field limit, present the Fraunhöfer and Fresnel-type analyses, and explore analytically how the bunch parameters affect the diffraction signal. In Sec. V we review a Gaussian model[17] for the electron bunch distribution, present sample numerical calculations of the diffraction signal, and further elaborate on the role of the bunch parameters and draw model-independent conclusions. Extra mathematical details are given in Appendixes A and C.

## II. THE WIGNER FUNCTION AND ITS VARIANCES

For the $N$-electron bunch we begin by introducing the single-particle Wigner function

$$W(\mathbf{u},\mathbf{p};t) = \int \frac{d^3r'}{(2\pi\hbar)^3} e^{i\mathbf{p}\cdot\mathbf{r}'/\hbar}\, \mathrm{Tr}[\rho_N \psi^\dagger(\mathbf{u}+\mathbf{r}'/2,t) \times \psi(\mathbf{u}-\mathbf{r}'/2,t)], \tag{1}$$

where $\rho_N$ is the $N$-particle density operator and $\psi(\mathbf{u},t)$ is the field operator associated with the annihilation of an electron at position $\mathbf{u}$ at time $t$. From $W(\mathbf{u},\mathbf{p};t)$ we can calculate the expectation values of all single-particle operators. In particular, the expectation value $n(\mathbf{u},t)$ of the density operator at $\mathbf{u}$ is given by

$$n(\mathbf{u},t) \equiv \int d^3p\, W(\mathbf{u},\mathbf{p};t) = \mathrm{Tr}[\rho_N \psi^\dagger(\mathbf{u},t)\psi(\mathbf{u},t)], \tag{2}$$

while the expectation value $\tilde{n}(\mathbf{p},t)$ of the density operator at momentum $\mathbf{p}$ is given by

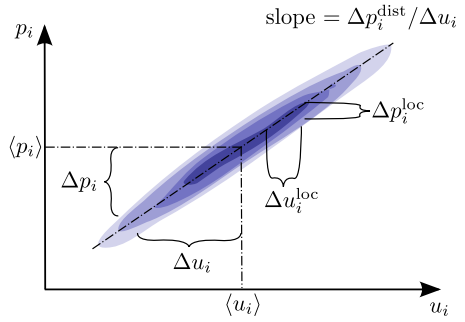


FIG. 2. (Color online) A phase-space picture of a distribution function showing some of the characteristic parameters. The index $i$ is a coordinate label.

$$\tilde{n}(\mathbf{p},t) \equiv \int d^3u\, W(\mathbf{u},\mathbf{p};t) = \mathrm{Tr}[\rho_N \tilde{\psi}^\dagger(\mathbf{p},t)\tilde{\psi}(\mathbf{p},t)], \tag{3}$$

where

$$\tilde{\psi}(\mathbf{p},t) = \int \frac{d^3r}{(2\pi\hbar)^{3/2}} e^{-i\mathbf{p}\cdot\mathbf{r}/\hbar}\psi(\mathbf{r},t) \tag{4}$$

is the field operator associated with the annihilation of an electron with momentum $\mathbf{p}$ at time $t$. Clearly

$$\int d^3u\, n(\mathbf{u},t) = \int d^3p\, \tilde{n}(\mathbf{p},t) = N. \tag{5}$$

In the absence of any vector potential the expectation value $\mathbf{j}(\mathbf{u},t)$ of the number current density operator is given by

$$\begin{aligned}\int d\mathbf{p}\frac{\mathbf{p}}{m} W(\mathbf{u},\mathbf{p};t) &= \int \frac{d^3p d^3u'}{(2\pi\hbar)^3} \mathrm{Tr}[\rho_N \psi^\dagger(\mathbf{r}+\mathbf{u}'/2,t)\psi(\mathbf{r}+\mathbf{u}'/2,t)] \\ &\times \frac{\partial}{\partial \mathbf{u}'}\left(\frac{\hbar}{im} e^{i\mathbf{p}\cdot\mathbf{u}'/\hbar}\right) \\ &= \mathrm{Tr}\left[\rho_N \psi^\dagger(\mathbf{u},t)\left(\frac{\hbar}{2mi}\nabla\right)\psi(\mathbf{u},t) + \mathrm{h.c.}\right] \equiv \mathbf{j}(\mathbf{u},t),\end{aligned} \tag{6}$$

where in moving from the first to the second line we have integrated by parts and used the fact that the particle density vanishes far from the bunch center.

The phase-space density of electron bunches in UED experiments is sufficiently low that while the electron bunch is freely propagating, or propagating in slowly varying electric and magnetic fields as it is directed toward the target, $W(\mathbf{u},\mathbf{p};t)$ can be associated with an effective classical distribution function $f(\mathbf{u},\mathbf{p};t)$; that is, $W(\mathbf{u},\mathbf{p};t)$ is non-negative for all values of its arguments. We can then introduce six parameters that describe the different variances of the momentum and position variables of $W(\mathbf{u},\mathbf{p};t)$, as sketched in Fig. 2. These variances will depend on time, as $W(\mathbf{u},\mathbf{p};t)$ evolves, but for simplicity we keep the time variable implicit in the expressions below.

To define the variances we begin with the average position and momentum of the electrons,

TABLE I. (A) Typical values of UED experimental parameters. (B) Typical parameters for 30 keV electron bunches. The variances are calculated for an electron bunch time of flight of 0.5 ns, with an initial bunch size of $\Delta u_T = 50\ \mu$m and $\Delta u_z = 0.13\ \mu$m, and a momentum spread corresponding to $\Delta E = 0.6$ eV (full width at half maximum). The label $T$ indicates any direction in the $(xy)$ plane, and the average velocity is in the $z$ direction.

| (A) UED experimental parameter values | | |
|---|---|---|
| Distance from target to detector | $r$ | 10–20 cm |
| Typical electron energy | $E = p^2/2m$ | 30–60 keV |
| Typical electron wavelength | $\lambda = 2\pi\hbar/p$ | 0.05–0.1 Å |

| (B) Parameter values for a 30 keV electron bunch at time of scattering | | | |
|---|---|---|---|
| $\Delta u_T = 100\ \mu$m | $\Delta u_z = 300\ \mu$m | $\Delta u_T^{\mathrm{loc}} = 45\ \mu$m | $\Delta u_z^{\mathrm{loc}} = 20\ \mu$m |
| $\Delta p_T/\hbar = 1000/\mu$m | $\Delta p_z/\hbar = 1000/\mu$m | $\Delta p_T^{\mathrm{loc}}/\hbar = 450/\mu$m | $\Delta p_z^{\mathrm{loc}}/\hbar = 60/\mu$m |

$$\langle \mathbf{u} \rangle = \frac{1}{N}\int d^3u \mathbf{u} n(\mathbf{u}) = \frac{1}{N}\int d^3u d^3p \mathbf{u} W(\mathbf{u},\mathbf{p}),$$

$$\langle \mathbf{p} \rangle = \frac{1}{N}\int d^3p \mathbf{p} \tilde{n}(\mathbf{p}) = \frac{1}{N}\int d^3u d^3p \mathbf{p} W(\mathbf{u},\mathbf{p}). \tag{7}$$

We also introduce an average position associated with a momentum $\mathbf{p}$, $\langle \mathbf{u}^{\mathrm{loc}}(\mathbf{p}) \rangle$, and an average momentum associated with a position $\mathbf{u}$, $\langle \mathbf{p}^{\mathrm{loc}}(\mathbf{u}) \rangle$, according to

$$\langle \mathbf{u}^{\mathrm{loc}}(\mathbf{p}) \rangle = \frac{1}{\tilde{n}(\mathbf{p})}\int d^3u \mathbf{u} W(\mathbf{u},\mathbf{p}),$$

$$\langle \mathbf{p}^{\mathrm{loc}}(\mathbf{u}) \rangle = \frac{1}{n(\mathbf{u})}\int d^3p \mathbf{p} W(\mathbf{u},\mathbf{p}). \tag{8}$$

We refer to these as the local means. The full variances for position and momentum are defined in the usual way,

$$(\Delta u_i)^2 = \frac{1}{N}\int d^3u d^3p W(\mathbf{u},\mathbf{p})(u_i - \langle u_i \rangle)^2,$$

$$(\Delta p_i)^2 = \frac{1}{N}\int d^3u d^3p W(\mathbf{u},\mathbf{p})(p_i - \langle p_i \rangle)^2, \tag{9}$$

where $i$ labels a Cartesian component. We also introduce variances $\Delta u_i^{\mathrm{loc}}$ and $\Delta p_i^{\mathrm{loc}}$,

$$(\Delta u_i^{\mathrm{loc}})^2 = \frac{1}{N}\int d^3u d^3p W(\mathbf{u},\mathbf{p})(u_i - \langle u_i^{\mathrm{loc}}(\mathbf{p}) \rangle)^2,$$

$$(\Delta p_i^{\mathrm{loc}})^2 = \frac{1}{N}\int d^3u d^3p W(\mathbf{u},\mathbf{p})(p_i - \langle p_i^{\mathrm{loc}}(\mathbf{u}) \rangle)^2. \tag{10}$$

The first is an average over the bunch of how much the position associated with a given momentum varies about its local mean; the second is an average over the bunch of how much the momentum associated with a given position varies about its local mean. Finally, we introduce the variances $\Delta u_i^{\mathrm{dist}}$ and $\Delta p_i^{\mathrm{dist}}$,

$$(\Delta u_i^{\mathrm{dist}})^2 = \frac{1}{N}\int d^3u d^3p W(\mathbf{u},\mathbf{p})(\langle u_i^{\mathrm{loc}}(\mathbf{p}) \rangle - \langle u_i \rangle)^2,$$

$$(\Delta p_i^{\mathrm{dist}})^2 = \frac{1}{N}\int d^3u d^3p W(\mathbf{u},\mathbf{p})(\langle p_i^{\mathrm{loc}}(\mathbf{u}) \rangle - \langle p_i \rangle)^2, \tag{11}$$

which characterize how much the local means vary throughout the bunch. These variances are not all independent. In fact, we find

$$(\Delta u_i)^2 = (\Delta u_i^{\mathrm{loc}})^2 + (\Delta u_i^{\mathrm{dist}})^2,$$

$$(\Delta p_i)^2 = (\Delta p_i^{\mathrm{loc}})^2 + (\Delta p_i^{\mathrm{dist}})^2, \tag{12}$$

for any function $W(\mathbf{u},\mathbf{p})$; hence there are four independent variances for each Cartesian component, two associated with position and two with momentum. In UED experiments the electron bunches are designed to have cylindrical symmetry about the direction of propagation, which we take as the $z$ axis. Hence $\Delta u_x^\nu = \Delta u_y^\nu \equiv \Delta u_T^\nu$ and $\Delta p_x^\nu = \Delta p_y^\nu \equiv \Delta p_T^\nu$, where $\nu$ indicates the local, distribution, or total variance. For this symmetry there are then eight independent parameters in all. In Table I we give typical values for these variances at the time of scattering as calculated by an analytic model,[17] based on experimental parameters found by Siwick *et al.*[3]

## III. THE SCATTERED ELECTRON CURRENT

For an interacting bunch of electrons it is impossible to find a closed system of dynamical equations for $W(\mathbf{u},\mathbf{p};t)$. Rather, a set of reduced distribution functions can be introduced, of which $W(\mathbf{u},\mathbf{p};t)$ is the first, which satisfy a hierarchy of coupled equations, as is the case for any general $N$-body problem. However, in UED experiments the electron bunch has typically expanded so much by the time it reaches the target that, when scattering occurs, the Coulomb repulsion between the electrons can be neglected. That is, the electrons see only the potential $V(\mathbf{r})$ responsible for their scattering; we consider this potential time independent, but our results can easily be extended to the more general case. In this stage of an UED experiment, the Wigner function satisfies the dynamical equation[18]

$$\frac{\partial W(\mathbf{u},\mathbf{p};t)}{\partial t} = -\frac{\mathbf{p}}{m}\cdot\frac{\partial W(\mathbf{u},\mathbf{p};t)}{\partial \mathbf{u}} + \frac{2}{\hbar}\sin\left(\frac{\hbar}{2}\frac{\partial}{\partial \mathbf{p}}\cdot\frac{\partial}{\partial \mathbf{u}}\right)V(\mathbf{u})W(\mathbf{u},\mathbf{p};t) \tag{13}$$

and the higher terms involving powers of $\hbar$ are crucial, since

they capture the quantum nature of the scattering.

Consider now a different problem, the description of a single electron system characterized by a density operator $\rho(t)$ acting over the Hilbert space of a single particle. Its Wigner function is given by

$$\bar{W}(\mathbf{u},\mathbf{p};t) = \int \frac{d^3u'}{(2\pi\hbar)^3} e^{i\mathbf{p}\cdot\mathbf{u}'/\hbar} \langle \mathbf{u}-\mathbf{u}'/2|\rho(t)|\mathbf{u}+\mathbf{u}'/2\rangle$$
$$= \int \frac{d^3p'}{(2\pi\hbar)^3} e^{i\mathbf{p}'\cdot\mathbf{u}/\hbar} \langle \mathbf{p}+\mathbf{p}'/2|\rho(t)|\mathbf{p}-\mathbf{p}'/2\rangle, \tag{14}$$

where $|\mathbf{u}\rangle$ are the single-particle position eigenkets and $|\mathbf{p}\rangle$ are the single-particle momentum eigenkets,

$$\langle \mathbf{u}|\mathbf{u}'\rangle = \delta(\mathbf{u}-\mathbf{u}'),$$

$$\langle \mathbf{p}|\mathbf{p}'\rangle = \delta(\mathbf{p}-\mathbf{p}'),$$

with

$$|\mathbf{p}\rangle = \int \frac{d^3u}{(2\pi\hbar)^{3/2}} e^{i\mathbf{p}\cdot\mathbf{u}/\hbar}|\mathbf{u}\rangle.$$

If the single electron is subject to the potential $V(\mathbf{r})$ introduced above, then the equation satisfied by $\bar{W}(\mathbf{u},\mathbf{p};t)$ is the same as Eq. (13). Of course, while $W(\mathbf{u},\mathbf{p};t)$ is normalized to $N$ [see Eqs. (2), (3), and (5)], $\bar{W}(\mathbf{u},\mathbf{p};t)$ is normalized to unity. However, since Eq. (13) is linear in the Wigner function we can remove this trivial difference by scaling up the trace of $\rho$ to be $N$ rather than unity,

$$\mathrm{Tr}[\rho(t)] \equiv \int d^3u \langle \mathbf{u}|\rho(t)|\mathbf{u}\rangle = \int d\mathbf{p}\langle \mathbf{p}|\rho(t)|\mathbf{p}\rangle = N.$$

Thus we can solve the many-body problem specified by Eq. (13) in single-particle language. At some initial time $t_{\mathrm{init}}$ we introduce a single-particle density operator

$$\rho(t_{\mathrm{init}}) = \int\int d^3p_1 d^3p_2 |\mathbf{p}_2\rangle\langle \mathbf{p}_2|\rho(t_{\mathrm{init}})|\mathbf{p}_1\rangle\langle \mathbf{p}_1|,$$

according to the inverse of Eq. (14) with $\bar{W}(\mathbf{u},\mathbf{p};t_{\mathrm{init}})$ taken to be our actual Wigner function $W(\mathbf{u},\mathbf{p};t_{\mathrm{init}})$,

$$\langle \mathbf{p}_2|\rho(t_{\mathrm{init}})|\mathbf{p}_1\rangle = \int d^3u e^{-i(\mathbf{p}_2-\mathbf{p}_1)\cdot\mathbf{u}/\hbar} W\left(\mathbf{u}, \frac{1}{2}(\mathbf{p}_1+\mathbf{p}_2); t_{\mathrm{init}}\right). \tag{15}$$

Then, if we can solve the corresponding dynamical equation for $\rho(t)$,

$$i\hbar\frac{d\rho(t)}{dt} = \left[\frac{\mathbf{P}^2}{2m} + V(\mathbf{U}), \rho(t)\right], \tag{16}$$

where $\mathbf{U}$ and $\mathbf{P}$ are, respectively, the single-particle position and momentum operators, at some later time $t$ we can find $W(\mathbf{u},\mathbf{p};t)$ according to

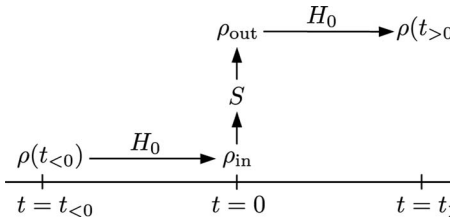


FIG. 3. A schematic view of the asymptotic-in and asymptotic-out scattering states. The free electron Hamiltonian is defined as $H_0 = \mathbf{P}^2/2m$.

$$W(\mathbf{u},\mathbf{p};t) = \int \frac{d^3p'}{(2\pi\hbar)^3} e^{i\mathbf{p}'\cdot\mathbf{u}/\hbar} \langle \mathbf{p}+\mathbf{p}'/2|\rho(t)|\mathbf{p}-\mathbf{p}'/2\rangle, \tag{17}$$

[cf. Eq. (14)].

We formulate the solution of Eq. (16) in terms of scattering theory.[19] We identify $t=0$ as the time the center of the electron bunch arrives at the target. We take an earlier time $t_{<0}$ to be well before the scattering process, and when the density operator $\rho(t_{<0})$ is subject to only the free electron Hamiltonian $H_0 = \mathbf{P}^2/2m$. We take $t_{>0}$ as a time well after the collision and when the density operator $\rho(t_{>0})$ is also subject to only $H_0$. The asymptotic-in density operator, $\rho_{\mathrm{in}}$, is the operator to which $\rho(t_{<0})$ evolves, from $t_{<0}$ to $t=0$, according to the free electron Hamiltonian $H_0$ (Fig. 3). Likewise, the operator $\rho(t_{>0})$ evolves from the asymptotic-out density operator $\rho_{\mathrm{out}}$, from $t=0$ to $t_{>0}$, according to the Hamiltonian $H_0$. The scattering process is then characterized by the scattering operator $S$,

$$\rho_{\mathrm{out}} = S\rho_{\mathrm{in}}S^\dagger, \tag{18}$$

where

$$S|\mathbf{p}\rangle = |\mathbf{p}\rangle + \frac{i}{2\pi\hbar m}\int d^3p'|\mathbf{p}'\rangle\delta(E'-E)f(\mathbf{p}\leftarrow\mathbf{p}'), \tag{19}$$

with $E = p^2/2m$ and where $f(\mathbf{p}\leftarrow\mathbf{p}')$ is the scattering amplitude associated with the potential $V(\mathbf{u})$. Any limitation of this description is solely due to approximations in determining the scattering amplitude from the scattering potential, which we discuss later.

Letting $t_{>0}=t$, the density operator $\rho(t)$ is given by $U_o(t)\rho_{\mathrm{out}}U_o^\dagger(t)$, where $U_o(t) = \exp(-iP^2t/(2m\hbar))$, and so

$$\langle \mathbf{p}_2|\rho(t)|\mathbf{p}_1\rangle = e^{-i(E_2-E_1)t/\hbar}\langle \mathbf{p}_2|\rho_{\mathrm{out}}|\mathbf{p}_1\rangle, \tag{20}$$

where $E_1 = p_1^2/2m$, etc. Using Eqs. (18) and (19) for $\rho_{\mathrm{out}}$ we can identify three contributions,

$$\rho_{\mathrm{out}} = \rho_0 + \rho_{\mathrm{hol}} + \rho_{\mathrm{diff}}, \tag{21}$$

where

$$\langle \mathbf{p}_2|\rho_0|\mathbf{p}_1\rangle = \langle \mathbf{p}_2|\rho_{\mathrm{in}}|\mathbf{p}_1\rangle, \tag{22a}$$

$$\langle \mathbf{p}_2|\rho_{\mathrm{hol}}|\mathbf{p}_1\rangle = \frac{i}{2\pi\hbar m}\times\left[\int d^3p_2'\delta(E_2'-E_2)f(\mathbf{p}_2\leftarrow\mathbf{p}_2')\times\langle\mathbf{p}_2'|\rho_{\mathrm{in},}|\mathbf{p}_1\rangle - \int d^3p_1'\delta(E_1'-E_1)\times\langle\mathbf{p}_2|\rho_{\mathrm{in}}|\mathbf{p}_1'\rangle f^*(\mathbf{p}_1\leftarrow\mathbf{p}_1')\right], \tag{22b}$$

$$\langle \mathbf{p}_2|\rho_{\mathrm{diff}}|\mathbf{p}_1\rangle = \frac{1}{(2\pi\hbar m)^2}\int d^3p_1'd^3p_2'\delta(E_2'-E_2)f(\mathbf{p}_2\leftarrow\mathbf{p}_2')\times\langle\mathbf{p}_2'|\rho_{\mathrm{in}}|\mathbf{p}_1'\rangle\delta(E_1'-E_1)f^*(\mathbf{p}_1\leftarrow\mathbf{p}_1'). \tag{22c}$$

Clearly $\rho_0$ describes the contribution of the outgoing signal that does not undergo scattering. The term $\rho_{\mathrm{hol}}$ describes a holography contribution, in that it captures the interference between the unscattered part of the bunch and the scattered part. Finally, $\rho_{\mathrm{diff}}$ describes the diffraction contribution, resulting from the interference of the scattered part of the bunch with itself.

In an UED experiment the measured quantity is the electron flux at a detector at position $\mathbf{r}$ at time $t$ (Fig. 1). We denote the flux through a solid angle $d\Omega$ in the direction $\hat{\mathbf{r}}$ at time $t$ as $\Gamma(\mathbf{r},t)$,

$$r^2\hat{\mathbf{r}}\cdot j(r,t)d\Omega \equiv \Gamma(\mathbf{r},t)d\Omega,$$

where $\mathbf{j}(\mathbf{r},t)$ is given by Eq. (6). Using the expression for the Wigner function Eq. (17), together with Eqs. (20), (21), and (22a)–(22c) for $\rho(t)$, we see that $\Gamma(\mathbf{r},t)$ can be written as the sum of three contributions; adopting an obvious notation, we write them as $\Gamma_0(\mathbf{r},t)$, $\Gamma_{\mathrm{hol}}(\mathbf{r},t)$, and $\Gamma_{\mathrm{diff}}(\mathbf{r},t)$. From the form of these equations we see that each of these terms, and thus the total $\Gamma(\mathbf{r},t)$, can be written in terms of two-energy functions, e.g.

$$\Gamma(\mathbf{r},t) = \int \frac{dE_1dE_2}{2\pi\hbar}\Gamma(\mathbf{r};E_1,E_2)e^{-i(E_2-E_1)t/\hbar}.$$

In UED experiments to date, it is the total, time-integrated signal $\Gamma(\mathbf{r})$ that is measured, which we also express as an integral over an energy dependent flux $\Gamma(\mathbf{r},E)\equiv\Gamma(\mathbf{r};E,E)$,

$$\Gamma(\mathbf{r}) \equiv \int dt\Gamma(\mathbf{r},t) = \int dE\Gamma(\mathbf{r},E).$$

As with $\Gamma(\mathbf{r},t)$, there are three contributions to $\Gamma(\mathbf{r},E)$; $\Gamma_0(\mathbf{r},E)$, $\Gamma_{\mathrm{hol}}(\mathbf{r},E)$, and $\Gamma_{\mathrm{diff}}(\mathbf{r},E)$, following our established notation.

To write the three components of $\Gamma(\mathbf{r},E)$ in a convenient form we henceforth use $W(\mathbf{u},\mathbf{p})$, with no time variable, to indicate the "asymptotic-in" Wigner function. That is, it would be the Wigner function of our electron bunch at $t=0$ were there no scattering potential. Then

$$\langle \mathbf{p}_2|\rho_{\mathrm{in}}|\mathbf{p}_1\rangle = \int d^3u e^{-i(\mathbf{p}_2-\mathbf{p}_1)\cdot\mathbf{u}/\hbar}W\left(\mathbf{u},\frac{1}{2}(\mathbf{p}_1+\mathbf{p}_2)\right), \tag{23}$$

[cf. Eq. (15)] and applying this relation to Eqs. (22a)–(22c) we find

$$\Gamma_0(\mathbf{r},E) = \frac{mp^2r^2}{(2\pi\hbar)^2}\hat{\mathbf{r}}\cdot\int d^3ud\hat{\mathbf{n}}_1d\hat{\mathbf{n}}_2\frac{1}{2}p(\hat{\mathbf{n}}_1+\hat{\mathbf{n}}_2)e^{i\mathbf{r}\cdot(\hat{\mathbf{n}}_2-\hat{\mathbf{n}}_1)p/\hbar}e^{-i\mathbf{u}\cdot(\hat{\mathbf{n}}_2-\hat{\mathbf{n}}_1)p/\hbar}W\left(\mathbf{u},\frac{1}{2}(\hat{\mathbf{n}}_1+\hat{\mathbf{n}}_2)p\right), \tag{24a}$$

$$\Gamma_{\mathrm{hol}}(\mathbf{r},E) = \frac{mp^3r^2}{(2\pi\hbar)^3}\hat{\mathbf{r}}\cdot\int d^3ud\hat{\mathbf{n}}_1d\hat{\mathbf{n}}_2d\hat{\mathbf{m}}\frac{1}{2}ip(\hat{\mathbf{n}}_1+\hat{\mathbf{n}}_2)e^{i\mathbf{r}\cdot(\hat{\mathbf{n}}_2-\hat{\mathbf{n}}_1)p/\hbar}e^{-i\mathbf{u}\cdot(\hat{\mathbf{m}}-\hat{\mathbf{n}}_1)p/\hbar}W\left(\mathbf{u},\frac{1}{2}(\hat{\mathbf{n}}_1+\hat{\mathbf{m}})p\right)f(p\hat{\mathbf{n}}_2\leftarrow p\hat{\mathbf{m}})+\mathrm{c.c.}, \tag{24b}$$

$$\Gamma_{\mathrm{diff}}(\mathbf{r},E) = \frac{mp^4r^2}{(2\pi\hbar)^4}\hat{\mathbf{r}}\cdot\int d^3ud\hat{\mathbf{n}}_1d\hat{\mathbf{n}}_2d\hat{\mathbf{m}}d\hat{\mathbf{l}}\frac{1}{2}p(\hat{\mathbf{n}}_1+\hat{\mathbf{n}}_2)e^{i\mathbf{r}\cdot(\hat{\mathbf{n}}_2-\hat{\mathbf{n}}_1)p/\hbar}e^{-i\mathbf{u}\cdot(\hat{\mathbf{m}}-\hat{\mathbf{l}})p/\hbar}W\left(\mathbf{u},\frac{1}{2}(\hat{\mathbf{l}}+\hat{\mathbf{m}})p\right)f(p\hat{\mathbf{n}}_2\leftarrow p\hat{\mathbf{m}})f^*(p\hat{\mathbf{n}}_1\leftarrow p\hat{\mathbf{l}}), \tag{24c}$$

where $p=\sqrt{2mE}$. These results are exact, within the approximation that the Coulomb interaction between the electrons is negligible in the scattering region, in which case Eq. (13) gives a good description of the electron dynamics.

## IV. DIFFRACTED FLUX IN THE FAR FIELD

Our focus is on the diffraction component of the flux, $\Gamma_{\mathrm{diff}}(\mathbf{r},E)$, which is of experimental interest. For current UED setups[3,20,21] the holographic component $\Gamma_{\mathrm{hol}}(\mathbf{r},E)$ is concentrated in the vicinity of the forward direction and is completely separated from the structure-dependent diffraction signal at the detection screen.

For thin film or few-molecule samples that are of interest in UED experiments, and at typical electron energies on the order of 30 keV, it is a good first approximation to assume that a single scattering event occurs from each atom in the target. The scattering amplitude can then be written as

$$f(\mathbf{p}_b\leftarrow\mathbf{p}_a) = \sum_j e^{-i\mathbf{R}_j\cdot(\mathbf{p}_b-\mathbf{p}_a)/\hbar}f_j(\mathbf{p}_b\leftarrow\mathbf{p}_a), \tag{25}$$

where the sum runs over all atoms $j$ with positions at $\mathbf{R}_j$, and where $f_j(\mathbf{p}_b\leftarrow\mathbf{p}_a)$ would be the scattering amplitude from atom $j$ were it located at the origin. For the rest of this paper we restrict ourselves to this approximation. Expression (24) for the diffraction can then be rewritten by introducing the momentum correlation function associated with the asymptotic-in Wigner function,

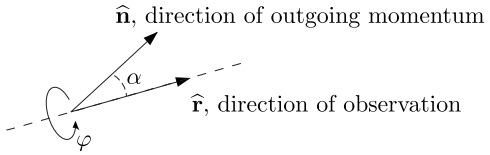


FIG. 4. Coordinates in Eq. (28) used in the far-field asymptotic approximation.

$$G(\mathbf{p}_1,\mathbf{p}_2) \equiv \int d^3u e^{-i(\mathbf{p}_2-\mathbf{p}_1)\cdot\mathbf{u}/\hbar} W\left(\mathbf{u},\frac{1}{2}(\mathbf{p}_1+\mathbf{p}_2)\right)$$

$$= \mathrm{Tr}[\rho_N \tilde{\psi}^\dagger(\mathbf{p}_1)\tilde{\psi}(\mathbf{p}_2)], \tag{26}$$

where we have used the defining expression (1) for the Wigner function and expression (4) for the momentum field operators. Note that in terms of our effective single-particle density operator (23) we have $G(\mathbf{p}_1,\mathbf{p}_2)=\langle\mathbf{p}_2|\rho_{\mathrm{in}}|\mathbf{p}_1\rangle$. Using Eqs. (25) and (26) in Eq. (24c), we have

$$\Gamma_{\mathrm{diff}}(\mathbf{r},E) = \frac{mp^4r^2}{(2\pi\hbar)^4}\hat{\mathbf{r}}\cdot\int d\hat{\mathbf{n}}_1 d\hat{\mathbf{n}}_2 d\hat{\mathbf{m}} d\hat{\mathbf{l}}\frac{1}{2}$$
$$\times p(\hat{\mathbf{n}}_1+\hat{\mathbf{n}}_2)G(p\hat{\mathbf{l}},p\hat{\mathbf{m}})$$
$$\times\sum_{j,k} e^{i\mathbf{r}\cdot(\hat{\mathbf{n}}_2-\hat{\mathbf{n}}_1)p/\hbar} e^{-ip\mathbf{R}_j\cdot(\hat{\mathbf{n}}_2-\hat{\mathbf{m}})/\hbar} e^{ip\mathbf{R}_k\cdot(\hat{\mathbf{n}}_2-\hat{\mathbf{l}})/\hbar}$$
$$\times f_j(p\hat{\mathbf{n}}_2\leftarrow p\hat{\mathbf{m}}) f_k^*(p\hat{\mathbf{n}}_1\leftarrow p\hat{\mathbf{l}}). \tag{27}$$

Further simplifications result for detectors in the far field. We first give a standard analysis of the far-field behavior of $\Gamma_{\mathrm{diff}}(\mathbf{r},E)$, and then give a more general analysis appropriate to UED experiments.

### A. A standard analysis

The integrals over the solid angles $\hat{\mathbf{n}}_1$ and $\hat{\mathbf{n}}_2$ in Eq. (27) are of the form

$$\int d\hat{\mathbf{n}} F(p\hat{\mathbf{n}}) e^{\pm ip\mathbf{r}\cdot\hat{\mathbf{n}}/\hbar} = \int d\mu d\varphi F(p\hat{\mathbf{n}}) e^{\pm irp\mu/\hbar}, \tag{28}$$

where $\mu=\cos\alpha$ (Fig. 4) and $F(p\hat{\mathbf{n}})$ includes sums of either terms $e^{-ip\mathbf{R}_j\cdot(\hat{\mathbf{n}}_2-\mathbf{m})/\hbar} f_j(p\hat{\mathbf{n}}_2\leftarrow p\hat{\mathbf{m}})$ or $e^{ip\mathbf{R}_k\cdot(\hat{\mathbf{n}}_1-\hat{\mathbf{l}})/\hbar} f_k^*(p\hat{\mathbf{n}}_1\leftarrow p\hat{\mathbf{l}})$, multiplied by unity or a prefactor involving $\hat{\mathbf{n}}$. If $p$ is a typical momentum magnitude for which $G(p\hat{\mathbf{l}},p\hat{\mathbf{m}})$ is significant, we have $rp/(2\pi\hbar)\gg 1$ for typical detection geometries. The rapid oscillation in the phase factor of Eq. (28) as $\mu$ varies from its end points at $\pm 1$ means that there will be little contribution from the integral over the range of $\mu$ except at those end points. The asymptotic expansion[22] for $rp/\hbar\to\infty$ is

$$\int d\hat{\mathbf{n}} F(p\hat{\mathbf{n}}) e^{irp\hat{\mathbf{r}}\cdot\hat{n}/\hbar}$$
$$\sim -i\frac{2\pi\hbar}{rp}[F(p\hat{\mathbf{r}})e^{irp/\hbar} - F(-p\hat{\mathbf{r}})e^{-irp/\hbar}], \tag{29}$$

and is valid as long as $F(p\hat{\mathbf{n}})$ varies little over the angle $\alpha$ on the order of the angular range $\theta_{\mathrm{osc}}=\sqrt{\hbar/(rp)}$ over which the oscillations in $e^{irp\hat{\mathbf{r}}\cdot\hat{\mathbf{n}}/\hbar}$ occur near the end points $\mu=\pm 1$; for typical experimental parameters (see Table I), $\theta_{\mathrm{osc}}\approx 10^{-5}$.

To confirm that Eq. (29) is valid we need to look at the range of solid angles $\hat{\mathbf{n}}_1$ and $\hat{\mathbf{n}}_2$ over which $e^{-ip\mathbf{R}_j\cdot(\hat{\mathbf{n}}_2-\mathbf{m})/\hbar} f_j(p\hat{\mathbf{n}}_2\leftarrow p\hat{\mathbf{m}})$ and $e^{ip\mathbf{R}_k\cdot(\hat{\mathbf{n}}_1-\hat{\mathbf{l}})/\hbar} f_k^*(p\hat{\mathbf{n}}_1\leftarrow p\hat{\mathbf{l}})$ vary for fixed $\hat{\mathbf{m}}$ and $\hat{\mathbf{l}}$; there clearly is no problem with the benign prefactor dependence on $\hat{\mathbf{n}}_1$ and $\hat{\mathbf{n}}_2$. The atomic scattering amplitudes themselves, $f_j(\mathbf{p}_b\leftarrow\mathbf{p}_a)$ and $f_k(\mathbf{p}_b\leftarrow\mathbf{p}_a)$, vary as the angle between $\mathbf{p}_a$ and $\mathbf{p}_b$ ranges on the order of the scattering angle $\vartheta_B$, where $\vartheta_B\approx\hbar/(a_Bp)$ is obtained from the Born approximation[19] and where $a_B$ is the Bohr radius. For typical energies (see Table I) we have $\vartheta_B\approx 10^{-2}$, satisfying $\vartheta_B\gg\theta_{\mathrm{osc}}$; hence when implementing Eq. (29) we are justified in setting $f_j(p\hat{\mathbf{n}}_2\leftarrow p\hat{\mathbf{m}})\approx f_j(p\hat{\mathbf{r}}\leftarrow p\hat{\mathbf{m}})$ and $f_k(p\hat{\mathbf{n}}_1\leftarrow p\hat{\mathbf{l}})\approx f_k(p\hat{\mathbf{r}}\leftarrow p\hat{\mathbf{l}})$.

Turning to the more sensitive phase factors, we need to be able to put $\exp(-ip\mathbf{R}_j\cdot\hat{\mathbf{n}}_2/\hbar)\approx\exp(-ip\mathbf{R}_j\cdot\hat{\mathbf{r}}/\hbar)$ and similarly for the term involving $\hat{\mathbf{n}}_1$. For a given $\hat{\mathbf{n}}_2$ we put $\hat{\mathbf{n}}_2=\hat{\mathbf{r}}\cos\alpha_2+\hat{\mathbf{t}}\sin\alpha_2$, where $\hat{\mathbf{t}}$ is some unit vector perpendicular to $\hat{\mathbf{r}}$; then we have exactly

$$e^{-ip\mathbf{R}_j\cdot\hat{\mathbf{n}}_2/\hbar} = e^{-ip\mathbf{R}_j\cdot\hat{\mathbf{r}}/\hbar} e^{-ip\mathbf{R}_j\cdot\hat{\mathbf{r}}(\cos\alpha_2-1)/\hbar} e^{-ip\mathbf{R}_j\cdot\hat{\mathbf{t}}\sin\alpha_2}.$$

To correctly implement the approximation (29), the second two exponentials on the right-hand side of the above equation must vary little as $\alpha_2$ varies over $\theta_{\mathrm{osc}}\approx 10^{-5}$. Putting $|\mathbf{R}_j\cdot\hat{\mathbf{r}}|\approx|\mathbf{R}_j\cdot\hat{\mathbf{t}}|\approx R_j$ and $\cos\alpha_2\approx 1-\alpha_2^2/2$, $\sin\alpha_2\approx\alpha_2$, we then require

$$\frac{R_j\theta_{\mathrm{osc}}^2p}{\hbar} = \frac{R_j}{r} \ll 1, \tag{30a}$$

$$\frac{R_j\theta_{\mathrm{osc}}p}{\hbar} = \frac{R_j}{r\theta_{\mathrm{osc}}} \ll 1. \tag{30b}$$

We can rewrite relation (30b) as

$$\frac{R_j^2}{r} \ll r\theta_{\mathrm{osc}}^2 \approx \lambda, \tag{31}$$

which is the standard Fraunhöfer diffraction condition.[23]

For a finite sample where $R_j$ is bounded, both of the above conditions can be satisfied if $r$ is taken large enough, and hence it is valid to implement the asymptotic expansion (29). Taking only the first term of Eq. (29) corresponding to the detector direction, Eq. (27) reduces to

$$\Gamma_{\mathrm{diff}}(\mathbf{r},E) \sim \frac{mp^3}{(2\pi\hbar)^2}\int d\hat{\mathbf{m}} d\hat{\mathbf{l}} G(p\hat{\mathbf{l}},p\hat{\mathbf{m}}) f(p\hat{\mathbf{r}}\leftarrow p\hat{\mathbf{m}})$$
$$\times f^*(p\hat{\mathbf{r}}\leftarrow p\hat{\mathbf{l}}), \tag{32}$$

where we have used Eq. (25) to write our result in terms of the full scattering amplitude. This result is given in terms of a general momentum correlation function $G(p\hat{\mathbf{l}},p\hat{\mathbf{m}})$, and thus is applicable to momentum correlation functions associated with a mixed effective single-particle density operator $\rho$ [Eq. (15)]. However, we can recover the usual result of scattering theory by taking $\rho$ to characterize a pure state,

$$\langle \mathbf{p}_1|\rho|\mathbf{p}_2\rangle = \tilde{\psi}(\mathbf{p}_1)\tilde{\psi}^*(\mathbf{p}_2),$$

where $\tilde{\psi}(\mathbf{p})$ is the momentum representation of the asymptotic-in wave function $\psi(\mathbf{r})$; from Eqs. (23) and (26) we find, for this special case, $G(p\hat{\mathbf{l}},p\hat{\mathbf{m}})=\tilde{\psi}^*(p\hat{\mathbf{l}})\tilde{\psi}(p\hat{\mathbf{m}})$, and

$$\Gamma_{\text{diff}}(\mathbf{r},E) \sim mp|\tilde{\psi}_{\text{sc}}(p\hat{\mathbf{r}})|^2,$$

where

$$\psi_{\text{sc}}(p\hat{\mathbf{r}}) = \frac{ip}{2\pi\hbar}\int d\hat{\mathbf{m}} f(p\hat{\mathbf{r}} \leftarrow p\hat{\mathbf{m}})\tilde{\psi}(p\hat{\mathbf{m}}),$$

which is a standard result from scattering theory.

However, the analysis leading to this familiar result requires an extension to treat UED experiments. Of the two conditions [(30a) and (30b)] used to find Eq. (32), the first is typically met in UED experiments (see Table I), but the second is not. For typical UED geometries, the inequality (30b) requires $R \ll 1$ $\mu$m, where $R$ is the distance from the origin to an atom in the sample. For an asymptotic-in electron bunch centered near even a large molecule this condition is satisfied; but in thin film geometries (see Fig. 5), the value of $R$ for a typical atom can be much larger than 1 $\mu$m. With the size of the incident bunch on the order of 100 $\mu$m, atoms in the sample that scatter an electron in the incident bunch will have an $R$ that will certainly violate condition (30b).

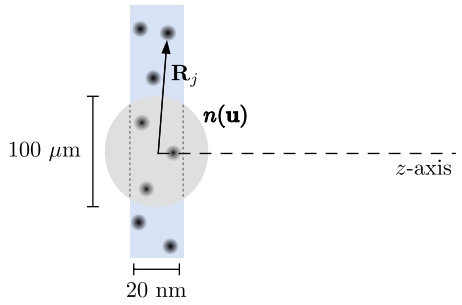


FIG. 5. (Color online) Thin film geometry. Sketched is the electron density $n(\mathbf{u})$ associated with $W_{\text{in}}(\mathbf{u},\mathbf{p})$. The transverse size of the electron bunch is on the order 100 $\mu$m, while the thin film can extend up to centimeters. The magnitude of $\mathbf{R}_j$, the coordinate of a typical atom, can take on values as large or greater than the size of the electron bunch.

A natural extension of the analysis presented above, which in the language of optics would be called "Fraunhöfer diffraction theory," would be to consider the more general Fresnel type of analysis. We return to Eq. (27) and rewrite it as

$$\Gamma_{\text{diff}}(\mathbf{r},E) = \frac{mp^4r^2}{(2\pi\hbar)^4}\hat{\mathbf{r}}\cdot\int d\hat{\mathbf{n}}_1 d\hat{\mathbf{n}}_2 d\hat{\mathbf{m}} d\hat{\mathbf{l}}\frac{1}{2}p(\hat{\mathbf{n}}_1+\hat{\mathbf{n}}_2)G(p\hat{\mathbf{l}},p\hat{\mathbf{m}})\sum_{j,k} e^{ip(\mathbf{r}-\mathbf{R}_j)\cdot\hat{\mathbf{n}}_2/\hbar}e^{-ip(\mathbf{r}-\mathbf{R}_k)\cdot\hat{\mathbf{n}}_1/\hbar}e^{ip(\mathbf{R}_j\cdot\hat{\mathbf{m}}-\mathbf{R}_k\cdot\hat{\mathbf{l}})/\hbar}f_j(p\hat{\mathbf{n}}_2 \leftarrow p\hat{\mathbf{m}})$$
$$\times f_k^*(p\hat{\mathbf{n}}_1 \leftarrow p\hat{\mathbf{l}}), \tag{33}$$

and then use the asymptotic expansion (29) with respect to the exponential now involving $(\mathbf{r}-\mathbf{R}_j)$ and $(\mathbf{r}-\mathbf{R}_k)$. So, for example, we reduce the integration over $\hat{\mathbf{n}}_2$ according to

$$\int d\hat{\mathbf{n}}_2 \bar{F}(p\hat{\mathbf{n}}_2)e^{ip(\mathbf{r}-\mathbf{R}_j)\cdot\hat{\mathbf{n}}_2/\hbar}$$
$$\sim -i\frac{2\pi\hbar}{|\mathbf{r}-\mathbf{R}_j|p}\bar{F}\left(p\frac{\mathbf{r}-\mathbf{R}_j}{|\mathbf{r}-\mathbf{R}_j|}\right)e^{i|\mathbf{r}-\mathbf{R}_j|p/\hbar}. \tag{34}$$

When the integral over $\hat{\mathbf{n}}_2$ is written in this form, the only quantities in $\bar{F}(p\hat{\mathbf{n}}_2)$ involving the solid angle $\hat{\mathbf{n}}_2$ are the scattering amplitude $f_j(p\hat{\mathbf{n}}_2 \leftarrow p\hat{\mathbf{m}})$ and $\hat{\mathbf{n}}_2$ itself. These vary slowly enough over $\theta_{\text{osc}}$, as discussed above, that Eq. (34) is clearly valid. However, the resulting expression is still complicated, and the usual strategy would be to begin by making the normally safe approximations,

$$\frac{1}{|\mathbf{r}-\mathbf{R}_j|} \approx \frac{1}{r},$$

$$\frac{\mathbf{r}-\mathbf{R}_j}{|\mathbf{r}-\mathbf{R}_j|} \approx \hat{\mathbf{r}},$$

$$f_j\left(p\frac{\mathbf{r}-\mathbf{R}_j}{|\mathbf{r}-\mathbf{R}_j|} \leftarrow p\hat{\mathbf{m}}\right) \approx f_j(p\hat{\mathbf{r}} \leftarrow p\hat{\mathbf{m}}), \tag{35}$$

and then expand the exponential term $e^{i|\mathbf{r}-\mathbf{R}_j|p/\hbar}$, going beyond the simple Fraunhöfer limit of $e^{ipr/\hbar}e^{-ip\hat{\mathbf{r}}\cdot\mathbf{R}_j/\hbar}$. Putting

$$|\mathbf{r}-\mathbf{R}_j| = \sqrt{r^2+R_j^2-2\mathbf{r}\cdot\mathbf{R}_j} = r\sqrt{1-2\frac{\hat{\mathbf{r}}\cdot\mathbf{R}_j}{r}+\frac{R_j^2}{r^2}}$$

and expanding, we find

$$\exp\left[\frac{ip}{\hbar}|\mathbf{r}-\mathbf{R}_j|\right]$$
$$= \exp\left[\frac{ip}{\hbar}\left(r-\hat{\mathbf{r}}\cdot\mathbf{R}_j+\gamma(\hat{\mathbf{r}},\mathbf{R}_j)+r\mathcal{O}\left(\frac{R_j^3}{r^3}\right)\right)\right], \tag{36}$$

where

$$\gamma(\hat{\mathbf{r}},\mathbf{R}_j) \equiv \frac{1}{2}\frac{R_j^2-(\hat{\mathbf{r}}\cdot R_j)^2}{r}$$

contains corrections to the phase beyond the Fraunhöfer approximation. If we can employ Eqs. (35) and (36), neglecting the order $R_j^3/r^3$ terms in the latter, we find

$$\Gamma_{\mathrm{diff}}(\mathbf{r},E) \sim \frac{mp^3}{(2\pi\hbar)^2}\int d\hat{\mathbf{m}}d\hat{\mathbf{l}}G(p\hat{\mathbf{l}},p\hat{\mathbf{m}}) \times \sum_j e^{-ip(\hat{\mathbf{r}}-\hat{\mathbf{m}})\cdot\mathbf{R}_j/\hbar}e^{ip\gamma(\hat{\mathbf{r}},\mathbf{R}_j)/\hbar}f_j(p\hat{\mathbf{r}}\leftarrow p\hat{\mathbf{m}}) \times \sum_k e_k^{ip(\hat{\mathbf{r}}-\hat{\mathbf{l}})\cdot\mathbf{R}_k/\hbar}e^{-ip\gamma(\hat{\mathbf{r}},\mathbf{R}_k)/\hbar}f_k^*(p\hat{\mathbf{r}}\leftarrow p\hat{\mathbf{l}}), \tag{37}$$

the Fresnel generalization of Eq. (32); here the sums over $j$ and $k$ cannot be performed in a simple way to yield the total scattering amplitudes because of the Fresnel factors.

Expression (37) requires for its justification the validity of Eq. (35) and the neglect of the $\mathcal{O}(R_j^3/r^3)$ terms in Eq. (36). Looking first at the second of these conditions, we would require

$$\frac{pr}{\hbar}\left(\frac{R_j^3}{r^3}\right) = \frac{1}{\theta_{\mathrm{osc}}^2}\left(\frac{R_j^3}{r^3}\right) \ll 1. \tag{38}$$

Even for atoms within the size of the electron bunch we can expect $R_j \approx 100\ \mu$m, and for $r \approx 10$ cm and $\theta_{\mathrm{osc}} \approx 10^{-5}$, we find

$$\frac{1}{\theta_{\mathrm{osc}}^2}\left(\frac{R_j^3}{r^3}\right) \approx 10,$$

and so the phase condition (38) is hardly satisfied. Thus even the Fresnel generalization [Eq. (37)] of Eq. (27) appears invalid.

In principle, of course, the situation appears even worse. One could imagine a thin film target where $R_j$ could range up to centimeters (see Fig. 5). For such atoms even the usually trivial conditions (35) will not be satisfied. Of course, such atoms are outside the range of the asymptotic-in electron bunch, and we physically expect them to make no contribution to the scattering. Nonetheless, a careful treatment of the diffracted signal should confirm this, rather than assume it. Such a careful treatment seems, from the analysis so far, to require the evaluation of the full Eq. (27).

In fact, the situation is not that bad. Up to this point we have not employed any of the properties of $G(p\hat{\mathbf{l}},p\hat{\mathbf{m}})$, or alternately of the Wigner function $W(\mathbf{u},\mathbf{p})$. The coherences of the electron bunch, as characterized by the variances of the Wigner function, are very limited. As a result, approximations can be made to Eq. (27) that are valid even in a careful treatment, simplifying the expression that must be evaluated to predict the diffracted signal. Another benefit of the more careful treatment we present below is that it allows us to identify how the variances, in fact, limit the performance of diffraction experiments made with the electron bunches they characterize. Once we use the coherence properties of $W(\mathbf{u},\mathbf{p})$ that describes the typical UED electron bunch, we find that Eq. (37) is, in fact, the correct form for the final expression of the diffraction signal.

### B. A more general analysis involving the role of bunch parameters

We begin by returning to Eq. (27) and, using Eq. (26), write it as

$$\Gamma_{\mathrm{diff}}(\mathbf{r},E) = \frac{mp^4r^2}{(2\pi\hbar)^4}\times\hat{\mathbf{r}}\cdot\int d\hat{\mathbf{n}}_1 d\hat{\mathbf{n}}_2 \frac{1}{2}p \times(\hat{\mathbf{n}}_1+\hat{\mathbf{n}}_2)e^{ip\mathbf{r}\cdot(\hat{\mathbf{n}}_2-\hat{\mathbf{n}}_1)/\hbar}\mathcal{F}(p\hat{\mathbf{n}}_1,p\hat{\mathbf{n}}_2), \tag{39}$$

where

$$\mathcal{F}(p\hat{\mathbf{n}}_1,p\hat{\mathbf{n}}_2) = \int d^3u d\hat{\mathbf{m}}d\hat{\mathbf{l}}e^{-i\mathbf{u}\cdot(\hat{\mathbf{m}}-\hat{\mathbf{l}})p/\hbar}W\left(\mathbf{u},\frac{1}{2}(\hat{\mathbf{l}}+\hat{\mathbf{m}})p\right)\sum_{j,k}e^{-ip\mathbf{R}_j\cdot(\hat{\mathbf{n}}_2-\hat{\mathbf{m}})/\hbar}e^{ip\mathbf{R}_k\cdot(\hat{\mathbf{n}}_1-\hat{\mathbf{l}})/\hbar}f_j(p\hat{\mathbf{n}}_2\leftarrow p\hat{\mathbf{m}})f_k^*(p\hat{\mathbf{n}}_1\leftarrow p\hat{\mathbf{l}}). \tag{40}$$

Using a change in variables detailed in Appendix A, without any approximations we can write Eq. (40) as

$$\mathcal{F}(p\hat{\mathbf{n}}_1,p\hat{\mathbf{n}}_2) = \frac{1}{p^2}\int d^3u d^2s d\hat{\mathbf{p}}W(\mathbf{u},p(s)\hat{\mathbf{p}})\sum_{j,k}e^{-i(\mathbf{u}-\mathbf{\Lambda}_{jk})\cdot\mathbf{s}/\hbar}e^{ip(s)\hat{\mathbf{p}}\cdot\mathbf{R}_{jk}/2\hbar}e^{-ip\mathbf{R}_{jk}\cdot(\hat{\mathbf{n}}_1+\hat{\mathbf{n}}_2)/2\hbar}e^{ip\mathbf{\Lambda}_{jk}\cdot(\hat{\mathbf{n}}_1-\hat{\mathbf{n}}_2)/\hbar} \times f_j(p\hat{\mathbf{n}}_2\leftarrow p(s)\hat{\mathbf{p}}-\mathbf{s})f_k^*(p\hat{\mathbf{n}}_1\leftarrow p(s)\hat{\mathbf{p}}+\mathbf{s}). \tag{41}$$

Here the two-dimensional vector $\mathbf{s}$ ranges over the plane perpendicular to a unit vector $\hat{\mathbf{p}}$ varying up to a magnitude of $2p$ (Fig. 6), $p(s)\equiv\sqrt{p^2-s^2/4}$, and

$$\mathbf{R}_{jk}\equiv\mathbf{R}_j-\mathbf{R}_k,$$

$$\mathbf{\Lambda}_{jk}\equiv\frac{1}{2}(\mathbf{R}_j+\mathbf{R}_k),$$

identify, respectively, the distance between two atomic sites $j$ and $k$, and the average position of the two sites.

We simplify expressions (39) and (41) on the basis of the following seven inequalities:

$$\theta_{\mathrm{osc}} \equiv \sqrt{\frac{\hbar}{rp}} \ll 1, \tag{42a}$$

$$\theta_{\mathrm{osc}} \ll \vartheta_B, \tag{42b}$$

$$\frac{\hbar}{\Delta u_T^{\mathrm{loc}}} \equiv p_Q^T \ll p, \tag{42c}$$

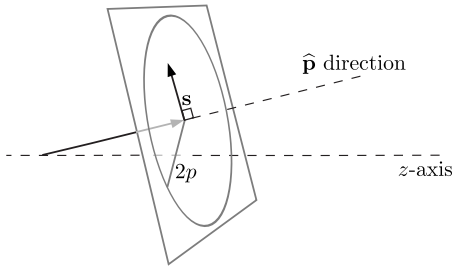


FIG. 6. Coordinates of integration of Eq. (41). The vector $\mathbf{s}$ ranges from 0 to $2p$ and remains strictly in the plane perpendicular to the $\hat{\mathbf{p}}$ direction.

$$p_Q^T \ll p\sqrt{\frac{\Delta p_z^{\mathrm{loc}}}{p}}, \tag{42d}$$

$$p_Q^T \ll p\,\vartheta_B, \tag{42e}$$

$$\frac{\max[\Delta u_T^2, w^2]}{r^2} \ll \frac{\lambda}{w}, \tag{42f}$$

$$\Delta p_{T,z} \ll p, \tag{42g}$$

where $p$ is the magnitude of a typical electron momentum, $\lambda = h/p$ is a typical electron de Broglie wavelength, and $w$ is the scattering sample width. These are all satisfied for typical UED electron bunches, as can be confirmed from the values in Table I. The relations (42a)–(42g) are not all independent; for example, if $\vartheta_B \ll 1$ and $\sqrt{\Delta p_z/p} \ll 1$ the relation (42c) follows from the validity of Eq. (42d) or (42e). However, we give all the relations here so that the validity of our results can be evaluated for future diffraction studies, perhaps with electron bunches qualitatively different than those currently used. The physics of Eqs. (42a) and (42b) has already been discussed: the condition $\theta_{\mathrm{osc}} \ll 1$ results from a large detector distance $r$ and bunch momentum $p$, which limits a scattered momentum component, with direction $\hat{\mathbf{n}}$, to be near parallel to the $\hat{\mathbf{r}}$ direction at the detector (Fig. 7). The inequality (42b) requires that this angle is much smaller than the angle over which the atomic scattering amplitudes vary significantly. The physics of the other inequalities will be identified as we use them in our simplification of Eqs. (39) and (41), on which we now embark.

We begin that simplification by examining the integral over $\mathbf{u}$ in Eq. (41). This integral will make a very small contribution unless $s \lesssim p_Q^T$, where $p_Q^T \equiv \hbar/\Delta u_T^{\mathrm{loc}}$ is the momentum associated with the variance in the local position of the electrons at a given $p$; for if $s$ is larger than $p_Q^T$ the phase

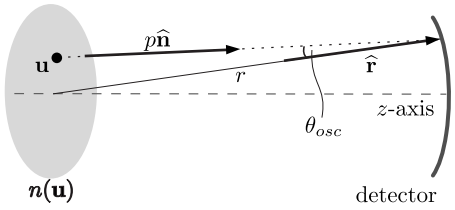


FIG. 7. An electron at a position $\mathbf{u}$ within the electron bunch has an outgoing scattered momentum $p\hat{\mathbf{n}}$. The angle $\theta_{\mathrm{osc}}$ between $\hat{\mathbf{n}}$ and the direction of observation $\hat{\mathbf{r}}$ is small if the distance to the detector $r$ is large [Eq. (42a)].

factor $\exp(i\mathbf{u}\cdot\mathbf{s}/\hbar)$ will vary as a function of $\mathbf{u}$ more quickly than $W(\mathbf{u}, p(s)\hat{\mathbf{p}})$ varies in $\mathbf{u}$, and no contribution will survive. Since $p_Q^T \ll p$ from Eq. (42c), we can then write $p(s) \equiv \sqrt{p^2 - s^2/4} \approx p - s^2/8p$ for the range of $s$ that will contribute. Relation (42d) is equivalent to $(p_Q^T)^2/2p \ll \Delta p_z^{\mathrm{loc}}$, and so for $s \lesssim p_Q^T$, we have $|p(s) - p| \ll \Delta p_{T,z}^{\mathrm{loc}}$; thus we can put $W(\mathbf{u}, p(s)\hat{\mathbf{p}}) \approx W(\mathbf{u}, p\hat{\mathbf{p}})$ since $W(\mathbf{u}, p(s)\hat{\mathbf{p}})$ will vary little over the range of $s$ for a fixed position $\mathbf{u}$. Finally, using Eq. (42e) and the fact that the atomic scattering amplitudes vary only as the angle between the two momenta varies over $\vartheta_B$, we see that we can put $f_j(p\hat{\mathbf{n}}_2 \leftarrow p(s)\hat{\mathbf{p}} - \mathbf{s}) \approx f_j(p\hat{\mathbf{n}}_2 \leftarrow p\hat{\mathbf{p}})$ and $f_k^*(p\hat{\mathbf{n}}_1 \leftarrow p(s)\hat{\mathbf{p}} + \mathbf{s}) \approx f_k^*(p\hat{\mathbf{n}}_1 \leftarrow p\hat{\mathbf{p}})$. In all, then, we can write

$$\mathcal{F}(p\hat{\mathbf{n}}_1, p\hat{\mathbf{n}}_2) = \frac{1}{p^2}\int d^3u d^2s d\hat{\mathbf{p}} W(\mathbf{u}, p\hat{\mathbf{p}}) \sum_{j,k} e^{i(\mathbf{u}-\mathbf{\Lambda}_{jk})\cdot\mathbf{s}/\hbar} \times e^{ip\hat{\mathbf{p}}\cdot\mathbf{R}_{jk}/2\hbar} e^{-ip\mathbf{R}_{jk}\cdot(\hat{\mathbf{n}}_1+\hat{\mathbf{n}}_2)/2\hbar} e^{-ip\mathbf{\Lambda}_{jk}\cdot(\hat{\mathbf{n}}_1-\hat{\mathbf{n}}_2)/\hbar} \times f_j(p\hat{\mathbf{n}}_2 \leftarrow p\hat{\mathbf{p}}) f_k^*(p\hat{\mathbf{n}}_1 \leftarrow p\hat{\mathbf{p}}). \tag{43}$$

Now although the integral over $\mathbf{s}$ ranges out to a maximum value of $2p$, relations (42c) and (42d) further limit the range over which $s$ contributes to $s \lesssim p_Q^T \ll 2p$, allowing us to extend the range of integration over $\mathbf{s}$ in Eq. (43) to infinity without introducing significant error. We then find

$$\mathcal{F}(p\hat{\mathbf{n}}_1, p\hat{\mathbf{n}}_2) = \frac{(2\pi\hbar)^2}{p^2}\int d^3u d\hat{\mathbf{p}} W(\mathbf{u}, p\hat{\mathbf{p}}) \sum_{j,k} \delta_{2D}^{\hat{\mathbf{p}}}(\mathbf{\Lambda}_{jk} - \mathbf{u}) \times e^{ip\hat{\mathbf{p}}\cdot\mathbf{R}_{jk}/2\hbar} e^{-ip\mathbf{R}_{jk}\cdot(\hat{\mathbf{n}}_1+\hat{\mathbf{n}}_2)/\hbar} e^{-ip\mathbf{\Lambda}_{jk}\cdot(\mathbf{n}_1-\mathbf{n}_2)/\hbar} \times f_j(p\hat{\mathbf{n}}_2 \leftarrow p\hat{\mathbf{p}}) f_k^*(p\hat{\mathbf{n}}_1 \leftarrow p\hat{\mathbf{p}}), \tag{44}$$

where $\delta_{2D}^{\hat{\mathbf{p}}}(\mathbf{r})$ indicates a two-dimensional delta function that vanishes unless the component of $\mathbf{r}$ perpendicular to $\hat{\mathbf{p}}$ is zero. Thus, the delta function $\delta_{2D}^{\hat{\mathbf{p}}}(\mathbf{\Lambda}_{jk} - \mathbf{u})$ in Eq. (44) forces $\mathbf{u}$ and $\mathbf{\Lambda}_{jk}$ to have equal components in the plane shown in Fig. 6. Using result (44) in expression (39) for $\Gamma_{\mathrm{diff}}(\mathbf{r}, E)$, we have

$$\Gamma_{\mathrm{diff}}(\mathbf{r}, E) = \frac{mp^2 r^2}{(2\pi\hbar)^2}\hat{\mathbf{r}} \cdot \int d\hat{\mathbf{n}}_1 d\hat{\mathbf{n}}_2 d^3u d\hat{\mathbf{p}} \frac{1}{2} p(\hat{\mathbf{n}}_1 + \hat{\mathbf{n}}_2) e^{ip\mathbf{r}\cdot(\hat{\mathbf{n}}_2-\hat{\mathbf{n}}_1)/\hbar} W(\mathbf{u}, p\hat{\mathbf{p}}) \sum_{j,k} \delta_{2D}^{\hat{\mathbf{p}}}(\mathbf{\Lambda}_{jk} - \mathbf{u}) \times e^{ip\hat{\mathbf{p}}\cdot\mathbf{R}_{jk}/2\hbar} e^{-ip\mathbf{R}_{jk}\cdot(\hat{\mathbf{n}}_1+\hat{\mathbf{n}}_2)/\hbar} e^{-ip\mathbf{\Lambda}_{jk}\cdot(\hat{\mathbf{n}}_1-\hat{\mathbf{n}}_2)/\hbar} f_j(p\hat{\mathbf{n}}_2 \leftarrow p\hat{\mathbf{p}}) f_k^*(p\hat{\mathbf{n}}_1 \leftarrow p\hat{\mathbf{p}}). \tag{45}$$

Let us pause now in our reduction in $\Gamma_{\mathrm{diff}}(\mathbf{r},E)$ and see what we can learn from this expression about the atomic sites that will contribute to the diffracted signal. From the delta function $\delta^{\hat{\mathbf{p}}}_{2D}(\mathbf{\Lambda}_{jk}-\mathbf{u})$ we see that only certain pairs of atoms $(j,k)$ will contribute. For the scattering centers that contribute, the component of $\mathbf{\Lambda}_{jk}$ perpendicular to $\hat{\mathbf{p}}$ must be within the distribution as defined by $W(\mathbf{u},p\hat{\mathbf{p}})$. Recalling relation (42g) and the fact that the average bunch momentum is along the $z$ axis, a $\hat{\mathbf{p}}$ within $W(\mathbf{u},p\hat{\mathbf{p}})$ is close to the $z$ axis. This means that the projection of $\mathbf{\Lambda}_{jk}$ is onto the $(xy)$ plane and must be within $\Delta u_T$ of the electron bunch for the pair of atoms $(j,k)$ to make a contribution to the diffraction signal; this is of course not surprising. Taking the center of the electron bunch to be at the origin, this condition is

$$\Lambda^T_{jk} \lesssim \Delta u_T, \tag{46}$$

where $\Lambda^T_{jk}$ is the magnitude of the projection of $\mathbf{\Lambda}_{jk}$ on the $(xy)$ plane.

The position difference between a pair of atoms $(j,k)$ also appears in the phase factors of expression (49). If the separation $\mathbf{R}_{jk}$ is so large that the phase varies greatly as the integrations over $\hat{\mathbf{p}}$ and $\hat{\mathbf{n}}$ are performed, there will be no net contribution to the integral. Hence there is a restriction on which pairs of atoms will give significant contributions, and since the effective range of integration over $\hat{\mathbf{p}}$ depends on the Wigner function, that restriction will depend on the momentum dependence of $W(\mathbf{u},\mathbf{p})$. The conditions restricting the size of $\mathbf{R}_{jk}$ can be used to simplify some of the terms in Eq. (49), and we begin by identifying those conditions.

The phase factor $\exp(-i\mathbf{R}_{jk}\cdot\mathbf{p}/\hbar)$ can be written in terms of transverse and longitudinal components of $\mathbf{R}_{jk}$. Putting $\mathbf{R}_{jk}=\mathbf{R}^T_{jk}+\hat{\mathbf{z}}R^z_{jk}$, where $R^z_{jk}=\hat{\mathbf{z}}\cdot\mathbf{R}_{jk}$, and similarly $\mathbf{p}=\mathbf{p}_T+\hat{\mathbf{z}}p_z$, with $p_z=\hat{\mathbf{z}}\cdot\mathbf{p}$, we have $\exp(-i\mathbf{R}_{jk}\cdot\mathbf{p}/\hbar)=\exp(-i\mathbf{R}^T_{jk}\cdot\mathbf{p}_T/\hbar)\exp(-iR^z_{jk}p_z/\hbar)$. Considering now the integrand in Eq. (49) for a fixed $\mathbf{u}$, recall that associated with the Wigner function $W(\mathbf{u},\mathbf{p})$ is a local average momentum $\langle\mathbf{p}^{\mathrm{loc}}(\mathbf{u})\rangle$, defined by Eq. (8). The function $W(\mathbf{u},\mathbf{p})$ typically has significant magnitude only for the transverse component of $\mathbf{p}$ within the limits $p_T\approx\langle\mathbf{p}^{\mathrm{loc}}_T(\mathbf{u})\rangle\pm\Delta p^{\mathrm{loc}}_T$ and the longitudinal component of $\mathbf{p}$ within the limits $p_z\approx\langle p^{\mathrm{loc}}_z(\mathbf{u})\rangle\pm\Delta p^{\mathrm{loc}}_z$. Thus one might expect a significant contribution to integral (49) when the difference vector $\mathbf{R}_{jk}$, for a pair of atoms $(j,k)$, satisfies

$$|\mathbf{R}^T_{jk}| \lesssim \frac{\hbar}{\Delta p^{\mathrm{loc}}_T}, \tag{47a}$$

$$|R^z_{jk}| \lesssim \frac{\hbar}{\Delta p^{\mathrm{loc}}_z}, \tag{47b}$$

or else the phase factor $\exp(-i\mathbf{R}_{jk}\cdot\mathbf{p}/\hbar)$ would lead to oscillations rapid enough for any contribution to vanish. However, this analysis is too simple. The quantities $\mathbf{p}_T$ and $p_z$ do not vary independently in the integration in Eq. (45), for that integration is at a fixed electron energy $E$ and therefore a fixed magnitude of the total momentum; only the direction $\hat{\mathbf{p}}$ is integrated over. As we see below, while condition (47a) is correct, condition (47b) is, in general, much too restrictive.

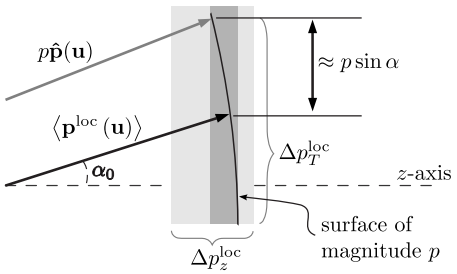


FIG. 8. The gray vector $p\hat{\mathbf{p}}(\mathbf{u})$ is the maximum possible variation of the average local momentum vector $\langle\mathbf{p}^{\mathrm{loc}}(\mathbf{u})\rangle$. This variation is limited by the local widths of the Wigner function $W(\mathbf{u},\mathbf{p})$. The actual variation of the $z$ component of the vector $\langle\mathbf{p}^{\mathrm{loc}}(\mathbf{u})\rangle$ for a fixed energy $E=p^2/2m$, denoted by the dark gray strip, is much less than $\Delta p^{\mathrm{loc}}_z$. The vector $p\hat{\mathbf{p}}(\mathbf{u})$ makes an angle $\alpha$ with $p\hat{\mathbf{p}}(\mathbf{u})$, while $\langle\mathbf{p}^{\mathrm{loc}}(\mathbf{u})\rangle$ makes an angle $\alpha_0$ with the $z$ axis.

At a fixed position $\mathbf{u}$, we take the average local momentum $\langle\mathbf{p}^{\mathrm{loc}}(\mathbf{u})\rangle$ to make an angle $\alpha_0$ with the $z$ axis, as sketched in Fig. 8. Since the full variation of the transverse component of the momentum over the bunch is characterized by $\Delta p_T$, the angle $\alpha_0$ satisfies $\alpha_0\leq\Delta p_T/p\ll 1$, where the second inequality follows from Eq. (42g). Next let us consider the range over which $p\hat{\mathbf{p}}$ can vary and still allow for a significant value of $W(\mathbf{u},p\hat{\mathbf{p}})$. If we indicate by $\alpha$ the maximum angle between $p\hat{\mathbf{p}}$ and $\langle\mathbf{p}^{\mathrm{loc}}(\mathbf{u})\rangle$ for which we can still get a significant contribution, we have $\alpha\approx|\Delta p^{\mathrm{loc}}_T/p|\ll 1$, where the inequality follows from Eq. (42g) and the fact that necessarily $\Delta p^{\mathrm{loc}}_T<\Delta p_T$ [see the second of Eq. (12)].

We can now consider for which pairs of atoms $(j,k)$ the phase factors $\exp(-i\mathbf{R}^T_{jk}\cdot\mathbf{p}_T/\hbar)\exp(-iR^z_{jk}p_z/\hbar)$ will change minimally over the variation of $\mathbf{p}_T$ and $p_z$ so that a contribution to integral (45) will survive. As the angle between $p\hat{\mathbf{p}}$ and $\langle\mathbf{p}^{\mathrm{loc}}(\mathbf{u})\rangle$ varies over a range $\alpha$, the maximum variation in the transverse component of $p\hat{\mathbf{p}}$ is $\delta p_T\approx p\sin\alpha\approx\Delta p^{\mathrm{loc}}_T$, while the maximum variation of the $z$ component of $p\hat{\mathbf{p}}$ is $\delta p_z\approx p[\cos(\alpha+\alpha_0)-\cos\alpha_0]\approx p(\alpha_0\alpha+\alpha^2/2)\approx\Delta p^{\mathrm{loc}}_T(\Delta p_T+\Delta p^{\mathrm{loc}}_T)/p$, where we keep only orders of magnitude in our estimates. We then see that as $p\hat{\mathbf{p}}$ varies over the range for which the Wigner function will allow a significant contribution, the phase factor $\exp(-i\mathbf{R}_{jk}\cdot\mathbf{p}/\hbar)=\exp(-i\mathbf{R}^T_{jk}\cdot\mathbf{p}_T/\hbar)\exp(-iR^z_{jk}p_z/\hbar)$ has a small enough variation for a contribution to survive as long as

$$|\mathbf{R}^T_{jk}| \lesssim \frac{\hbar}{\delta p_T} \approx \frac{\hbar}{\Delta p^{\mathrm{loc}}_T} \equiv L_T, \tag{48a}$$

$$|R^z_{jk}| \lesssim \frac{\hbar}{\delta p_z} \approx \frac{p\hbar}{\Delta p^{\mathrm{loc}}_T(\Delta p_T+\Delta p^{\mathrm{loc}}_T)} \equiv L_z, \tag{48b}$$

where $L_T$ and $L_z$ play the role of coherence lengths, respectively, transverse and parallel to the average velocity of the bunch. The asymmetry in the form of these two lengths arises because typical momenta in the distribution, which has its average momentum in the $z$ direction, are much larger than either the longitudinal or transverse momentum spreads [Eq. (42g)]. For typical parameters in current experiments (see Table I), we have $\Delta p^{\mathrm{loc}}_T\ll\Delta p_T$, and so, in fact, $L_z\approx p\hbar/(\Delta p^{\mathrm{loc}}_T\Delta p_T)$; with thin film thicknesses typically on the order of $w\approx 20$–$40$ nm we have $L_z\gg w$, and there is essentially no restriction on the pairs of atoms that can contribute

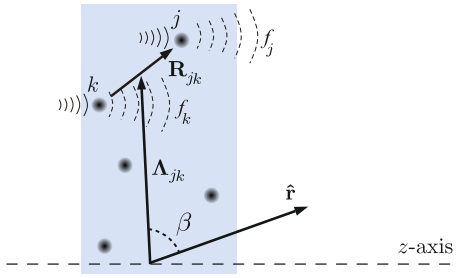


FIG. 9. (Color online) Detail of angles defined in Eq. (49) and a simple sketch of the Huygens–Fresnel principle. The solid lines represent the incident electron waves and the dashed lines represent the scattered electron waves.

to the diffraction signal due to their separation in $z$.

With the restrictions on the interatomic separation identified, we now proceed in simplifying Eq. (45). We proceed with far-field approximations of the $\hat{\mathbf{n}}_1$ and $\hat{\mathbf{n}}_2$ integrals according to Eq. (34), which sets $\hat{\mathbf{n}}_1=(\mathbf{r}-\mathbf{R}_k)/|\mathbf{r}-\mathbf{R}_k|$ and $\hat{\mathbf{n}}_2=(\mathbf{r}-\mathbf{R}_j)/|\mathbf{r}-\mathbf{R}_j|$. Relation (42b) and $r \gg R_j, R_k$ lets us set $\hat{\mathbf{n}}_1=\hat{\mathbf{n}}_2=\hat{\mathbf{r}}$ in the atomic scattering factors $f_j(p\hat{\mathbf{n}} \leftarrow p\hat{\mathbf{p}})$.

After the far-field approximations, the phases contain terms proportional to $|\mathbf{r}-\mathbf{R}_j|$ and $|\mathbf{r}-\mathbf{R}_k|$. These terms are then expanded for small $r/R_j$ (and for small $r/R_k$) as $|\mathbf{r}-\mathbf{R}_j| \approx r(1-\mathbf{R}_j \cdot \hat{\mathbf{r}}/r+\cdots)$. The restrictions on $\mathbf{R}_{jk}$ and $\mathbf{\Lambda}_{jk}$ now allow us to simplify the combined phase factors and neglect terms of order $O(1/r^2)$ and higher, the details of which are in Appendix B. The result of the approximations is the simplified expression

$$\Gamma_{\mathrm{diff}}(\mathbf{r},E) \sim \frac{mp^3r^2}{(2\pi\hbar)^2}\int d\hat{\mathbf{p}}d^3u W(\mathbf{u},p\hat{\mathbf{p}}) \times \sum_{j,k} \delta^{\hat{\mathbf{p}}}_{2D}(\mathbf{\Lambda}_{jk}-\mathbf{u}) e^{-i\mathbf{R}_{jk}\cdot(p\hat{\mathbf{r}}-p\hat{\mathbf{p}})/\hbar} \times e^{ip\sin^2\beta \mathbf{R}_{jk}\cdot\mathbf{\Lambda}_{jk}/\hbar r} f_j(p\hat{\mathbf{r}} \leftarrow p\hat{\mathbf{p}}) f_k^*(p\hat{\mathbf{r}} \leftarrow p\hat{\mathbf{p}}), \tag{49}$$

where $\hat{\mathbf{R}}_j \cdot \hat{\mathbf{r}} \approx \hat{\mathbf{R}}_k \cdot \hat{\mathbf{r}} \approx \hat{\mathbf{\Lambda}}_{jk} \cdot \hat{\mathbf{r}} \approx \sin\beta$ (Fig. 9). Our final expression (49) is equivalent to the previously derived Eq. (37), where we find that

$$\gamma(\hat{\mathbf{r}},\mathbf{R}_j) - \gamma(\hat{\mathbf{r}},\mathbf{R}_k) \approx \frac{1}{r}\mathbf{R}_{jk} \cdot \mathbf{\Lambda}_{jk} \sin^2\beta. \tag{50}$$

Our simplifications from Eqs. (47)–(50) have relied on the fact that only contributions from atom pairs with interatomic distances within the coherence lengths $L_T$ and $L_z$ will sum coherently, and that only atoms within the bunch size $\Delta u_T$ will contribute to the calculated signal. A concern might be that our simplifications, while treating the atoms that do contribute correctly, could inadvertently lead to an incorrect contribution in Eq. (50) of atoms that do not contribute in the more exact Eq. (47a). However, one can confirm that this is not so; the simpler Eq. (50) gives the correct result for all atoms, as long as our bunch satisfies the properties Eq. (42).

The details of the formation of diffraction patterns will be discussed in the Sec. V, but we give a qualitative analysis now. While the local momentum spread of the Wigner function imposes limitations on the separation $\mathbf{R}_{jk}$ of atoms contributing to the diffraction pattern, as we have seen above, the diffraction pattern formed by scattered electrons, and its salient features, are determined by the sum over atomic pairs in Eq. (49). Here the high energy of the bunch electrons again plays an important role. The scattering amplitude $f_j(p\hat{\mathbf{r}} \leftarrow p\hat{\mathbf{p}})$ in the integrand of Eq. (49) limits the range over which the scattering varies to an angle $\vartheta_B \approx 10^{-2}$. Hence, for an atom pair $(j,k)$ with $\mathbf{R}_{jk}=(\mathbf{R}^T_{jk},R^z_{jk})$, the role of the different components $R^T_{jk}$ and $R^z_{jk}$ on the diffraction pattern are considerably different. The $R^T_{jk}$-related contribution in the phase is on the order of $R^T_{jk}p\vartheta_B/\hbar$ and can vary considerably when $R^T_{jk}$ changes by one interatomic distance. Since $(\hat{\mathbf{r}}-\hat{\mathbf{p}})_z \approx \vartheta_B^2$, the $R^z_{jk}$-related contribution in the phase is on the order of $R^z_{jk}p\vartheta_B^2/\hbar$, a very slow function of $R^z_{jk}$. For this reason, the characteristic features of the shape of the diffraction pattern are formed by the summation over $R^T_{jk}$, while the summation over $R^z_{jk}$ contributes mainly to the overall intensity. Furthermore, we recall the restriction $R^T_{jk} \lesssim L_T$ [Eq. (48)]. For typical bunch parameters this gives $L_T \approx 20$ Å, which is larger then the interatomic distances in molecules and solids. Therefore, one would expected that this limited coherence of the bunches will reduce the visibility of the diffraction pattern, but not smear it completely.

Finally, we note that Eq. (49) can be seen as a manifestation of the Huygens–Fresnel principle in the electron optics of partially coherent bunches interacting with molecules and solids, as sketched in Fig. 9. Here the bunch Wigner function $W(\mathbf{u},p\hat{\mathbf{p}})$ at the target corresponds to the local intensity of the incident wave at the point $\mathbf{u}=\mathbf{\Lambda}_{jk}$ at the sample surface, and the interfering partially coherent secondary waves, produced by the incident wave, form the diffraction pattern $\Gamma_{\mathrm{diff}}(\mathbf{r},E)$.

## V. DIFFRACTION PATTERNS FOR GAUSSIAN BUNCHES

### A. Gaussian model

Having simplified the diffracted flux to the final expression (49), we would like to evaluate it for realistic bunches used in UED experiments. This requires a knowledge of the asymptotic-in state of the electron bunch $W(\mathbf{u},\mathbf{p})$, as well as the form of the atomic scattering amplitude. We first address the form of $W(\mathbf{u},\mathbf{p})$.

In an earlier paper[17] we introduced a simple and very accurate model of electron bunch propagation that assumes a Gaussian phase-space distribution to describe the bunch. We assume this same Gaussian form here for $W(\mathbf{u},\mathbf{p})$, which lets us further simplify Eq. (49). The simplification provides an expression amenable to numerical calculations where the physics is clearly seen, and also characterizes the diffraction expression in terms of parameters that fully describe the electron bunch at the time of scattering.

Using the variance parameters defined in Sec. II and employing the cylindrical symmetry of the experimental setup, the form of the distribution is

$$W(\mathbf{u},\mathbf{p}) = C\exp\left[-\frac{x^2+y^2}{2\Delta u_T^2}-\frac{z^2}{2\Delta u_z^2}\right] \times\exp\left[-\frac{(p_x-\chi_T x)^2+(p_y-\chi_T y)^2}{2(\Delta p_T^{\mathrm{loc}})^2}\right] \times\exp\left[-\frac{(p_z-p_0-\chi_z z)^2}{2(\Delta p_z^{\mathrm{loc}})^2}\right], \quad (51)$$

where $\chi_i=\Delta p_i^{\mathrm{dist}}/\Delta u_i$, $i=T$ or $z$, and $C$ is the normalization constant,

$$C=\frac{N}{(2\pi)^3}\frac{1}{\Delta u_T^2\Delta u_z(\Delta p_T^{\mathrm{loc}})^2\Delta p_z^{\mathrm{loc}}}.$$

To evaluate Eq. (49) using the Gaussian form (51), we define the following $\hat{\mathbf{p}}$-dependent orthogonal coordinate system (Fig. 10)

$$\hat{\mathbf{e}}_1=\hat{\mathbf{x}}\cos\theta\cos\phi+\hat{\mathbf{y}}\cos\theta\sin\phi-\hat{\mathbf{z}}\sin\theta,$$

$$\hat{\mathbf{e}}_2=-\hat{\mathbf{x}}\sin\phi+\hat{\mathbf{y}}\cos\phi,$$

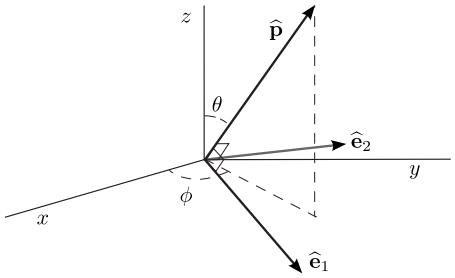


FIG. 10. New coordinate system (52) defined with respect to $\hat{\mathbf{p}}$, used in Eq. (53).

$$\hat{\mathbf{p}}=\hat{\mathbf{x}}\sin\theta\cos\phi+\hat{\mathbf{y}}\sin\theta\sin\phi+\hat{\mathbf{z}}\cos\theta, \quad (52)$$

and recall that $\mathbf{\Lambda}_{jk}\equiv(\mathbf{R}_j+\mathbf{R}_k)/2$ and $\mathbf{R}_{jk}\equiv\mathbf{R}_j-\mathbf{R}_k$. Even though the angle $\theta$ can take on any value between 0 and $\pi$, a significant contribution to integral (49) occurs only for the range of $\theta$ from 0 to $\Delta p_T/p$ due to the form of Eq. (51). Given the typical values of $\Delta p_T$ and $p$ (Table I), $\theta\lesssim 10^{-3}$ and we make the small angle approximation in the distribution function. Proceeding with the simplifications (Appendix C), the diffraction expression reduces to

$$\Gamma_{\mathrm{diff}}(\mathbf{r},E)=\frac{mp^3r^2}{(2\pi\hbar)^2}C\exp\left[-\frac{(p-p_0)^2}{(\Delta p_z^{\mathrm{loc}})^2}\right]\int d\hat{\mathbf{p}}A(\hat{\mathbf{z}}\cdot\hat{\mathbf{p}})\sum_{j,k}e^{-i\mathbf{R}_{jk}\cdot(p\hat{\mathbf{r}}-p\hat{\mathbf{p}})/\hbar}e^{ip\sin^2\beta\mathbf{R}_{jk}\cdot\mathbf{\Lambda}_{jk}/\hbar r} \times\exp\left[-\frac{(p\theta-\chi_T\mathbf{\Lambda}_{jk}\cdot\hat{\mathbf{e}}_1)^2}{2(\Delta p_T^{\mathrm{loc}})^2}-\frac{\chi_T^2(\mathbf{\Lambda}_{jk}\cdot\hat{\mathbf{e}}_2)^2}{2(\Delta p_T^{\mathrm{loc}})^2}\right]\exp\left[-\frac{(\mathbf{\Lambda}_{jk}\cdot\hat{\mathbf{e}}_1)^2+(\mathbf{\Lambda}_{jk}\cdot\hat{\mathbf{e}}_2)^2}{2\Delta u_T^2}\right]f_j(p\hat{\mathbf{r}}\leftarrow p\hat{\mathbf{p}})f_k^*(p\hat{\mathbf{r}}\leftarrow p\hat{\mathbf{p}}), \quad (53)$$

where the angles $\theta$ and $\beta$ are shown in Fig. 11, $p_0$ is the momentum associated with the average bunch energy, $p$ is associated with the chosen energy $E$, and $A$ is given by

$$A(\hat{\mathbf{z}}\cdot\hat{\mathbf{p}})=\sqrt{2\pi}\left[\frac{(\Delta p_z^{\mathrm{dist}})^2(\hat{\mathbf{z}}\cdot\hat{\mathbf{p}})^2}{(\Delta p_z^{\mathrm{loc}})^2\Delta u_z^2}+\frac{(\Delta p_T^{\mathrm{dist}})^2(1-(\hat{\mathbf{z}}\cdot\hat{\mathbf{p}})^2)}{(\Delta p_T^{\mathrm{loc}})^2\Delta u_T^2}\right]^{-1/2}.$$

Expression (53) confirms the role of the length scales $\Delta u_T$ and $L_T$ as discussed in Sec. IV B. The atoms that contribute to the diffraction signal are only those within the bunch size $\Delta u_T$, and the transverse coherence length $L_T\equiv\hbar/\Delta p_T^{\mathrm{loc}}$ is the length scale on which the transverse component of the phase factor sum coherently. As expected, expression (53) is not very sensitive to the $z$-related bunch parameters and depends on them only in a trivial way. Any limitations on the $z$ component of the phase, more precisely $z$ component of $\mathbf{R}_{jk}$, is strictly due the physical dimensions of the sample.

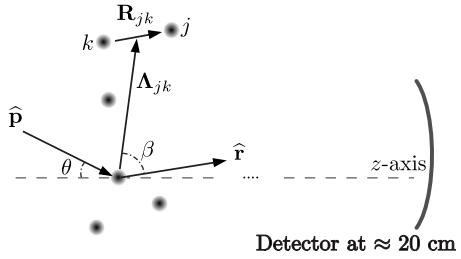


FIG. 11. The variables and geometry for Eq. (53).

### B. Numerical calculations and analysis of diffraction patterns

In this section we perform a sample analysis of the effects of the bunch properties on the diffraction patterns obtained in UED experiments. We consider ensembles of small scatterers, such as few-atom molecules and larger nanosize objects such as big molecules and crystal nanodomains. In general, the properties of the scatterers and the bunch are combined in the resulting diffraction pattern in a rather complex way, and their clear separation can be problematic. As we will see below, under typical experimental conditions the diffraction pattern of small molecules depends weakly on the bunch properties. However, for more extended objects the situation is different. There the interplay of possible constructive interference of the electron wave scattered by different atoms, and the local ($\Delta p_T^{\mathrm{loc}}$) and global ($\Delta p_T$) broadening of the bunch in momentum space, can lead to a

significant dependence of the pattern on the bunch properties. This effect is important for the analysis of the crystal structure and its time evolution in systems out of equilibrium.

Due to the high electron energies, the Born approximation can be applied to describe the single-atom scattering. For our sample calculations, the resulting scattering amplitude can be parametrized by a simple form[24] corresponding to the scattering by a screened Coulomb potential,

$$f_0(p\hat{\mathbf{r}} \leftarrow p\hat{\mathbf{p}}) = \frac{Ze^2}{4E} \frac{1}{\vartheta_B^2 + \sin^2(\theta/2)}, \tag{54}$$

where $\theta$ is the angle between $\hat{\mathbf{r}}$ and $\hat{\mathbf{p}}$, $Z$ is the nuclear charge, and $\vartheta_B$ is the characteristic Born scattering angle for a given atom, introduced in Sec. IV A. At angles $\theta \gg \vartheta_B$, $f_0(p\hat{\mathbf{r}} \leftarrow p\hat{\mathbf{p}})$ approaches the scattering amplitude of an electron by a point particle with the charge of the atomic nucleus. For many-electron atoms, the atomic form factor that determines the scattering amplitude, and correspondingly $\vartheta_B$, can be estimated with the Thomas–Fermi model. Within this approach the atomic cross section is $\sigma_{at} \approx a_B^2 Z^{3/2} \mathrm{Ry}/E$, where Ry is the Rydberg constant.

As the first example of electron bunch diffraction, we consider a small scatterer such as a molecule a few angstroms in size. The molecule is not characterized by a periodic structure, and therefore, constructive interference of the scattered waves on a scale larger than an interatomic distance, which could lead to well-defined Bragg peaks, does not arise (a complex detailed analysis of electron diffraction by small molecules in the case of plane waves can be found in Ref. 25). The scattering amplitude of the molecule is

$$f_{\mathrm{mol}}(p\hat{\mathbf{r}} \leftarrow p\hat{\mathbf{p}}) = \sum_j e^{-ip\mathbf{R}_j \cdot (\hat{\mathbf{r}} - \hat{\mathbf{p}})/\hbar} f_j(p\hat{\mathbf{r}} \leftarrow p\hat{\mathbf{p}}),$$

where the index $j$ runs over the atoms in the molecule. The heaviest atoms have the largest scattering amplitudes and give the strongest contribution to the scattering pattern. Since the typical interatomic distance between the atoms, $R_{jk}$, is on the order of 1 Å, the phases $p\mathbf{R}_{jk}(\hat{\mathbf{p}} - \hat{\mathbf{r}})/\hbar$ in the scattering amplitudes in Eq. (53) are on the order of one, and the scattering occurs at angles on the order of $\vartheta_B$ for the heaviest atoms in the molecule. The quantum mechanical scattering cross section by a single molecule, in the case the scattered electrons are described by the plane waves, is then given by

$$\sigma_{\mathrm{mol}}(p) = \int d\hat{\mathbf{p}} |f_{\mathrm{mol}}^2(p\hat{\mathbf{r}} \leftarrow p\hat{\mathbf{p}})|.$$

The cross section depends on the orientation of the molecule with respect to the incident beam, mainly due to the phases $p\mathbf{R}_j \cdot (\hat{\mathbf{r}} - \hat{\mathbf{p}})/\hbar$. The small size of a molecule, according to the estimate in Eq. (B4), allows us to neglect the phase $p \sin^2 \beta \mathbf{R}_{jk} \cdot \mathbf{\Lambda}_{jk}/\hbar r$ in Eq. (53), and therefore, to use the Fraunhöfer rather than the Fresnel approach for the scattering process.

We further analyze Eq. (53) by looking at electrons with a local mean momentum $\langle \mathbf{p}^{\mathrm{loc}}(\mathbf{R}) \rangle$ and a local momentum distribution characterized by $\Delta p_T^{\mathrm{loc}}$, arriving at a molecule located at an arbitrary point $\mathbf{R}$ within the electron bunch. In a gas, where the distance between molecules is much larger than the coherence length of the bunch, the resulting picture is the sum of randomly distributed spot intensities scattered by different molecules. From Eq. (53) two distinct limits for the scattering regimes by a small single molecule are possible, both of which depend on the bunch and scatterer properties. The first limit is *sharp scattering* with $\vartheta_B \ll \vartheta_{\mathrm{loc}}$, where $\vartheta_{\mathrm{loc}} \equiv \Delta p_T^{\mathrm{loc}}/p$. In this case $\hat{\mathbf{p}}$ and $\hat{\mathbf{r}}$ directions are close to each other, integration over the angle between $\hat{\mathbf{p}}$ and $\hat{\mathbf{r}}$ can be separated and yields the scattering cross section. As a result one obtains

$$\Gamma_{\mathrm{diff}}(\mathbf{r}, E) \approx A_{\mathrm{nar}} \sigma_{\mathrm{mol}}(p) \exp[-p^2 \theta_{\mathbf{R}}^2 / 2(\Delta p_T^{\mathrm{loc}})^2],$$

where $\theta_{\mathbf{R}}$ is the angle between $\langle \mathbf{p}^{\mathrm{loc}}(\mathbf{R}) \rangle$ and the direction to the observation point from the position of the molecule, and $A_{\mathrm{nar}}$ is an $\mathbf{r}$-independent constant determined by the bunch properties. In this case the diffraction pattern is bunch determined. The other limit is that of *broad scattering*, which arises if $\vartheta_B \gg \vartheta_{\mathrm{loc}}$. In this case the factors depending on the local momentum spread of the bunch can be integrated out leading to the result

$$\Gamma_{\mathrm{diff}}(\mathbf{r}, E) \approx A_{\mathrm{br}} |f_{\mathrm{mol}}(\theta_{\mathbf{R}})|^2,$$

where $A_{\mathrm{br}}$ is another $\mathbf{r}$-independent constant determined by the bunch properties. Here, the diffraction pattern produced by a few-atom single molecule is scatterer determined.

The case of broad scattering is more realistic for the bunches currently used in UED experiments, with $(\Delta p_T^{\mathrm{loc}})^2 \ll p_{\mathrm{at}}^2$, where $p_{\mathrm{at}} = \sqrt{2mR_y} = \hbar/a_B$ is the characteristic momentum of electron in an atom, than the sharp scattering. For example, the results of calculations done by Michalik and Sipe,[17] and summarized in Table I, show that $\Delta p_T^{\mathrm{loc}}$ corresponds to the energy spread $(\Delta p_T^{\mathrm{loc}})^2/2m$ of the order of 0.1 eV, limiting $\vartheta_{\mathrm{loc}}$ to about $10^{-3}$. This is an order of magnitude smaller than the angular spread of the electron bunch $\Delta p_T/p$ and the Born angle for the typical electron energies of the order of 50 keV, that is $\vartheta_B \gg \vartheta_{\mathrm{loc}}$.

For crystal or molecular structure analysis one is interested in the diffraction patterns produced by more extended periodic or quasiperiodic structures, where the scattering picture is more complicated than in the case of molecules, and a clear separation of the *sharp* and *broad* scattering limits, presented above, is often not possible. For extended objects, the crystal structure is characterized by the reciprocal lattice vectors $\mathbf{b}_j$. As a result, clear maxima in the scattered electron flux in the Bragg directions $\hat{\mathbf{r}}_B^{(j)}$ determined by

$$p(\hat{\mathbf{r}}_B^{(j)} - \hat{\mathbf{p}}) = \hbar \mathbf{b}_j, \tag{55}$$

are expected due to constructive interference. At electron energies larger than 10 keV the condition $p \gg \hbar b_j$ is satisfied for all experimentally interesting $\mathbf{b}_j$. The Bragg scattering occurs at small angles $\vartheta_{\mathrm{Bragg}}^{(j)} = \hbar b_j/p$, on the order of $10^{-2}$. Since we are interested in the scattering by polycrystalline samples, the Bragg peaks are transformed into Bragg circles. Were the incident electrons represented by plane waves, the width $\delta\vartheta_{\mathrm{Bragg}}^{(j)}$ of the Bragg peaks for nanocrystals, and correspondingly that of the circles for polycrystallines, would be determined by the diffraction limit of the nanocrystals. The diffraction-limited peak width satisfies the inequality

$\delta\vartheta^{(j)}_{\text{Bragg}} \sim \vartheta^{(j)}_{\text{Bragg}}/N_{\text{nc}} \ll \vartheta^{(j)}_{\text{Bragg}}$, where $N_{\text{nc}}$ is the number of atoms along the length of a nanocrystal. The diffraction patterns formed by realistic electron bunches can have broader diffraction peaks due to a more complex scattering process due to bunch properties.

To understand the role of the bunch properties on the diffraction pattern, we consider a system of large molecules or nanosize domains, uniformly but randomly distributed, oriented in a plane and scattering ultrafast electrons. The random in-plane position of one end of a molecule (one corner of a domain) is denoted by $\mathbf{R}_D$, while the orientation of its crystal axes is given by a pair of orthogonal vectors $(\mathbf{e}_1^{(D)}, \mathbf{e}_2^{(D)})$. The in-plane coordinates of the atoms in a domain are given by $\mathbf{R}_j = \mathbf{R}_D + a(n_1\mathbf{e}_1^{(D)} + n_2\mathbf{e}_2^{(D)})$, with integer $n_1$ and $n_2$, and $a$ the lattice constant, as shown in Fig. 12. The atomic coordinates are restricted by $0 \le n_1 \le N_1$ and $0 \le n_2 \le N_2$, where $N_1$ and $N_2$ determine the size of the nanodomain. The electron free path in a solid is on the order of $a^3/\sigma_{\text{at}}$. For biological molecules and light elements, such as aluminum, the Thomas–Fermi scattering cross section $\sigma_{\text{at}}$ can be used to estimate the electron mean-free path in the sample. This estimation yields a path distance hundreds of lattice constants, justifying the application of the single scattering approximation on nanoscale sized samples.

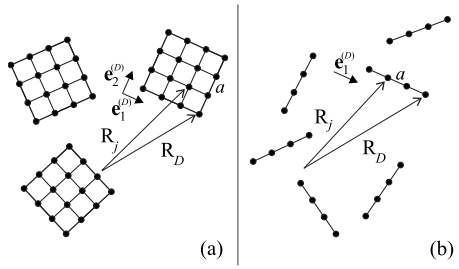


FIG. 12. Definition of the domain position $\mathbf{R}_D$ and the lattice cites $\mathbf{R}_j$ used in calculations of $\Gamma_{\text{diff}}$ in Eq. (56): (a) square lattices and (b) linear molecules.

The diffraction pattern is formed by the sum over molecules/domains $D$ with the contribution of the domain dependent on its position. Since the Bragg angles are small, we put $\beta = \pi/2$ in Eq. (53) and, following Appendix C1, obtain

$$\Gamma_{\text{diff}}(\mathbf{r},E) = \frac{mp^3r^2}{(2\pi\hbar)^2} CA(1)\exp\left[-\frac{(p-p_0)^2}{(\Delta p_z^{\text{loc}})^2}\right]\int d^2p_\perp \exp[-p_\perp^2/2(\Delta p_T)^2]$$
$$\times \sum_{\mathbf{R}_D} \exp[-(\mathbf{p}_\perp - \chi_T\mathbf{R}_D)^2/2(\Delta p_T^{\text{loc}})^2]|f_0(p\hat{\mathbf{r}} \leftarrow p\hat{\mathbf{p}})|^2 \left\langle \left| \sum_{n_1,n_2} \exp[ip\mathbf{d}_{n_1,n_2}(\hat{\mathbf{r}} - \hat{\mathbf{p}} - \mathbf{R}_D/r)/\hbar]\right|^2 \right\rangle, \quad (56)$$

where $p_\perp = (p_x, p_y)$, $\mathbf{d}_{n_1,n_2} = a(n_1\mathbf{e}_1^{(D)} + n_2\mathbf{e}_2^{(D)})$ goes over all atoms in the domain, and $C$ and $A(1)$ are normalization parameters introduced in Eq. (53). The angle brackets $\langle \ldots \rangle$ denote an average over the orientation of domains.

For random orientations of domains this averaging can be performed first. Then the incoherent contributions of different domains are summed up taking into account the $\mathbf{R}_D$ dependence of the bunch properties. The lattice sum has maxima at the Bragg directions leading to the maxima in $\Gamma_{\text{diff}}(\mathbf{r},E)$ at the corresponding scattering angles. For the Bragg circles, $\Gamma_{\text{diff}}(\mathbf{r},E)$ becomes a function of the distance from the position of the point hit by electron and the center of the detecting screen $r_s$, that is, $\Gamma_{\text{diff}}(\mathbf{r},E) \equiv \Gamma_{\text{diff}}(r_s,E)$ (Fig. 13). The maxima of $\Gamma_{\text{diff}}(r_s,E)$ are expected at $r_s = r_B^{(j)} \equiv r\hbar b_j/p$ $(j=1,2,\ldots)$. Since the distribution of momenta of electrons in the bunch have a very narrow spread, the positions of the maxima depend rather weakly on the bunch properties, while, as will be shown below, the width of the peaks can depend considerably on the bunch properties. As seen in Eq. (56), the entire diffraction pattern can depend on the transverse bunch coherence length $L_T = \hbar/\Delta p_T^{\text{loc}}$, which is of the order of few nanometers for typical UED bunches, on the momentum spread $\Delta p_T$ through the dependence of the direction of the momentum on the electron position in the bunch, and on the size of the crystallines from which the electrons diffract.

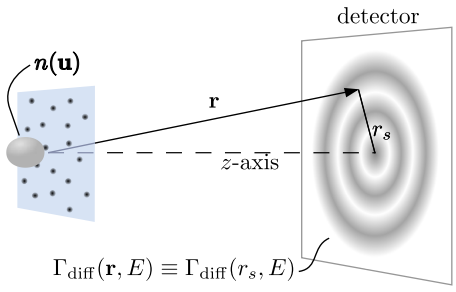


FIG. 13. (Color online) Definition of $r_s$.

To illustrate the effect of the bunch parameters and the scatterer geometry on the diffraction signal, we present some example calculations. We calculate the diffraction signals at an electron energy of 50 keV for two sample geometries, linear molecules and square nanocrystals, considering different values of the bunch parameters $\Delta p_T$, $\Delta p_T^{\text{loc}}$, and $\Delta u_T$. The values used for these parameters correspond to previous simulations[17] and are presented in the caption of Fig. 14. The main plots in Figs. 14(a) and 14(b) show the results obtained for large samples with a transverse size much larger than the bunch radius $\Delta u_T$. The insets show the scattered signal from small samples, with a size on the order of one micron, much less than $\Delta u_T$. The small samples, which are effectively illuminated by only part of the bunch, show narrow peaks in

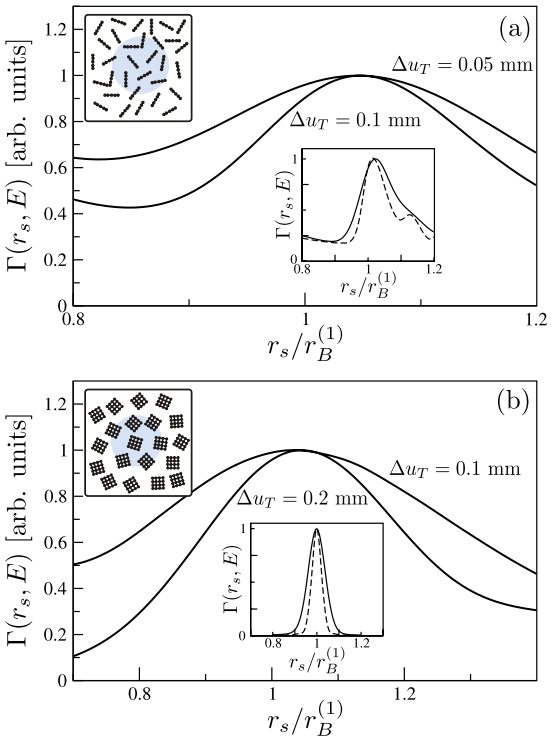


FIG. 14. (Color online) A sample numerical calculation of the diffracted signal using the final expression for $\Gamma(\hat{\mathbf{r}}, E)$ (53) and a Gaussian model for the Wigner distribution with an electron energy of 50 keV ($\lambda$=0.055 Å). Main plots: (a) $\Delta p_T = p/500$ and $L_T$=17 Å. The targets are linear clusters, 32 unit cells in length, unit cell 4 Å. (b) $\Delta p_T = p/250$ and $L_T$=17 Å. The targets are square clusters, 32×32 unit cells, unit cell 4 Å. Insets: $\Delta p_T = p/500$, narrow peak $L_T$=35 Å, wider peak $L_T$=17 Å. All other parameters are the same except the target radius is 1 $\mu$m in size. The local bunch spread $\Delta p_T^{\mathrm{loc}}/p = \lambda/2\pi L_T$ and the diffraction-limited Bragg spot width $\theta_{\mathrm{Bragg}}^{(1)}/N_{\mathrm{nc}}$ are of the same order of magnitude and both significantly to the width of the peaks in the insets.

comparison to the signal from the large samples. The diffraction signal for these small samples is broadened by both the local momentum distribution $\Delta p_T^{\mathrm{loc}}$, and the diffraction-limited momentum spread $\hbar b_j/N_{\mathrm{nc}}$, where $N_{\mathrm{nc}}$ is the order of $\max(N_1, N_2)$, and forms Bragg rings with a width on the order of $r\lambda/L_T$, where $L_T$ is defined in Eq. (48a). The signal from the large samples is also broadened by the global momentum width $\Delta p_T$.

An interesting feature of $\Gamma_{\mathrm{diff}}(r_s, E)$, illustrated in the inset of Fig. 14(a), is the slower decay at, and the shift of the maximum to, higher scattering angles compared to the scattering by domains with the square lattice structure. The reason for this distorted shape of the Bragg peak is the lower symmetry of the linear molecules. The random angular distribution leads to a distribution in the effective lattice constants seen in the diffraction pattern; all of them will be smaller than $a$. This effect shifts the effective Bragg vectors $b_j$ to larger values, and leads to the shift to larger $r_s$ and the asymmetry of the peak. We also mention the role the transverse bunch coherence, $L_T$, could play on changes in the scattered intensity if the shape of large molecules changes. For example, if the bond angles in an initially long, linear molecule were allowed to vary over a wide range, the molecule could be squeezed into an area with radius on the order $L/N_L^{1/2} \ll L$, where $L$ is the original length of the molecule

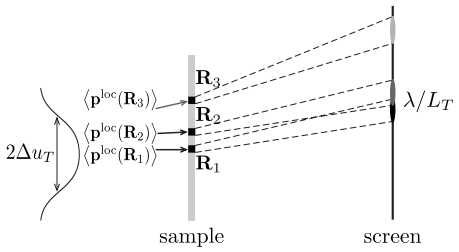


FIG. 15. The broadening of the diffraction peak. Only part of the diffraction picture is shown. The darkness of the elliptic spot corresponds to the signal intensity at the screen. Every cluster $\mathbf{R}_D$ is hit with a local mean electron momentum as shown in the figure. The Gaussian on the left-hand side shows the electron density distribution in the bunch.

and $N_L$ the number of atoms. If $L \geq L_T$ the electrons scattered by the linear molecule would not be spatially coherent, while the squeezed molecule would contain more atoms within an area of $L_T^2$ that could scattered electrons coherently. Thus, the scattering intensity would increase greatly.

The nature of broad peak formation is illustrated in Fig. 15 for arbitrary $\mathbf{R}_D$ positions ($\mathbf{R}_1$, $\mathbf{R}_2$, and $\mathbf{R}_3$). The electrons at the wings of the bunch produce scattering at higher angles with decreasing intensity and, therefore, lead to an inhomogeneous broadening of the Bragg peaks. As one can see in Eq. (56), the inhomogeneous broadening has two main contributions. First, a "geometrical" or "phase" contribution due to the factor $(\hat{\mathbf{r}} - \hat{\mathbf{p}} - \mathbf{R}_D/r)$ in the scattering phase of Eq. (56). The other, a "physical" contribution, is due to the $\langle \mathbf{p}^{\mathrm{loc}}(\mathbf{R}_D) \rangle$ dependence for the electrons arriving at the target. In other words, the Bragg spot moves both due to the change in the position of the scattering domain, and due to the change in the direction of the local momentum of the electrons hitting the domain. The distance between the first and second Bragg circles for the square nanodomains is $2\pi r\hbar(\sqrt{2}-1)/pa$, which is typically on the order of 1 mm. The peak broadening due to $\Delta p_T$ is on the order of $r\Delta p_T/p$ and can be a fraction of a millimeter or larger. In contrast to scattering by small molecules, discussed at the beginning of this subsection, scattering by an extended sample can be approximately described by one of the following three regimes for the Bragg peak broadening. These three regimes follow from Eq. (56).

In the first regime, the ring width $w$ on the screen is determined by the coherence of the bunch and the diffraction-limited scattering by nanodomains, and is on the order of $r \max(\lambda/L_T, \delta\vartheta_{\mathrm{Bragg}}^{(j)})$, providing the lower limit for the peak width, $w_{\mathrm{lim}}$. The conditions of this regime are $w_{\mathrm{lim}} > \Delta u_T$ and $w_{\mathrm{lim}} > r\Delta p_T/p$. A second regime occurs when the bunch size is increased so that $\Delta u_T > w_{\mathrm{lim}}$ and $\Delta u_T > r\Delta p_T/p$. The third regime is realized if the transverse momentum is sufficiently large such that $r\Delta p_T/p > w_{\mathrm{lim}}$ and $r\Delta p_T/p > \Delta u_T$. In the two latter cases, the peak width is approximately the maximum of either the bunch size $\Delta u_T$ (second regime) or $r\Delta p_T/p$ (third regime), arising due to the above mentioned "phase" and physical contributions, respectively. In the third regime, the peak width can be similar in size to the distance between the peaks corresponding to two close reciprocal lattice vectors, since the regime where $\Delta p_T$ and $\hbar b_j$ are comparable is a typical one.

There is an interesting feature of the third regime related to the role of the Born scattering angle on the peak broadening. Because the typical Bragg angle, Born scattering angle, and the angle characterizing the global spread of the bunch are all of the same order of magnitude, only a portion of the clusters in the sample can contribute significantly to a given Bragg peak, even those clusters with $R_D < \Delta u_T$. This can lead to the peak width depending on the bunch parameters in a more complex way than described in the previous paragraph. For example, in Fig. 14 we observe a decrease in the peak width with an increase of the bunch size $\Delta u_T$ for constant $\Delta p_T$. This occurs in the following way. For an arbitrary position $\mathbf{R}_D$, electrons with a large local transverse momentum component $\langle \mathbf{p}_T^{\mathrm{loc}}(\mathbf{R}_D)\rangle = \chi_T \mathbf{R}_D$ will be located closer to the wings of the bunch due to a linear transverse chirp, or equivalently, at relatively for large values of $R_D$. For an electron to arrive at the screen at the position of the first Bragg peak determined by the direction $\hat{\mathbf{r}}_B^{(1)}$ in Eq. (55), it should be scattered from $\langle \mathbf{p}^{\mathrm{loc}}(\mathbf{R}_D)\rangle$ to $p\hat{\mathbf{r}}_B^{(1)}$, that is, by an angle on the order of $\max(p_T^{\mathrm{loc}}(\mathbf{R}_D)/p, \vartheta_{\mathrm{Bragg}}^{(1)})$. For given $\mathbf{R}_D$, if $p_T^{\mathrm{loc}}(\mathbf{R}_D)/p$ is larger than the Born angle $\vartheta_B$, the contribution of this cluster to the diffraction flux in Eq. (56), will be considerably decreased by a small scattering amplitude $|f_0(p\hat{\mathbf{r}}_B^{(1)} \leftarrow \langle \mathbf{p}^{\mathrm{loc}}(\mathbf{R}_D)\rangle)|$ [Eq. (54)] even if $R_D < \Delta u_T$. Therefore, given two bunches with the same total momentum spread, a larger bunch can produce a diffraction pattern with narrower peak widths, as is the case in our sample calculation. Recall that the local momentum $\langle \mathbf{p}^{\mathrm{loc}}(\mathbf{R}_D)\rangle$ varies within $\Delta p_T^{\mathrm{loc}} < \Delta p \ll p$ as a function of $z$. Hence the above analysis is valid for any point $\mathbf{R}_D$ within the bunch.

Finally, we mention another possible contribution to the width of the Bragg rings formed by the diffracted electron bunches. Equation (53) describes scattering of electrons with a given absolute value of momentum $p$. However, the bunch includes electrons with a certain spread in the energy, and correspondingly in $p$. For the strongly anisotropic situation, where $p \gg \Delta p_z$ and $p \gg \Delta p_T$, the energy spread of the bunch is on the order of $p\Delta p_z/m$. This broadening, however, has almost no impact on the ring width. Indeed, as follows from Eq. (55), the finite $\Delta p_z$ of the bunch results in a relative broadening of the Bragg rings on the order of $\Delta p_z/p \approx 10^{-2}$, which is at least an order of magnitude smaller than the effect of the transverse momentum $\Delta p_T$ discussed above. This conclusion is independent of the Gaussian model for the bunch.

## VI. CONCLUSION

In this paper we have derived a general expression for the diffracted flux of electron bunches used in UED experiments. In our approach, the classical distribution that describes the electron bunch during propagation is associated at the target with the asymptotic-in Wigner function. We presented a far-field analysis of the diffraction expression appropriate for the experimental conditions, and investigated the effects of the bunch parameters on the diffraction signal, which lead to simplifications of the diffraction expression. The simplifications included a Fraunhöfer-type analysis that is valid for scattering from small objects such as molecules, and a more general Fresnel-type analysis that resulted in an expression appropriate for scattering from larger targets, such as thin films. The derived diffraction signal is expressed in terms of parameters that characterize the incident electron bunch, the atomic scattering amplitudes, and the crystal structure. This expression provides insight to how the properties of the incident bunch affect the observed diffraction pattern.

In our analysis of the diffraction expression we identified the bunch parameters that are important in the formation of the diffraction pattern. We found that the size of the bunch clearly limits which atoms contribute to the scattered signal, while $L_T = \hbar/\Delta p_T^{\mathrm{loc}}$, where $\Delta p_T^{\mathrm{loc}}$ is the local momentum spread in the transverse direction inside the bunch, plays the role of the transverse coherence length and is the length scale on which pairs of atoms contribute coherently. We also derived a $z$-coherence length $L_z$, related to $L_T$ through geometry and bunch properties. The length scale set by $L_z$, though, is much larger than the maximum $z$-direction atom separation in a typical experiment, and hence there are typically no restrictions in the longitudinal direction as there are in the transverse. Furthermore, for typical UED bunches we show that the diffraction expression is not sensitive to the $z$-direction parameters and that the slow variation in the $z$ component of the phase results in contributing mainly to the overall intensity of the diffraction pattern. We presented sample numerical calculations to quantify the effects of the bunch parameters and the effects of the target structure on the diffraction signal for Gaussian bunches.

Our results show that for small, molecule sized objects the diffraction pattern is scatterer determined. For large objects, the Bragg peaks are dependent on a complex interplay of the bunch and target properties, where a clear separation between the effects of the bunch and target parameters cannot be made. Our simulations do illustrate the changes in the Bragg peaks for different values of the parameters, for example, a decrease in peak width with an increase in the transverse bunch size $\Delta u_T$. Such simulations are important in understanding how the signal resolution will change for different electron bunches used in UED experiments.

Our derivation of the general scattering formalism for UED electron bunches also included an expression for a holographic signal. This holographic component of the scattered signal is insignificant for the experimental conditions of typical UED experiments. In a future publication we hope to apply a thorough analysis of this expression to explore the experimental conditions a holographic signal can be obtained for electron bunches.

## ACKNOWLEDGMENTS

We would like to thank R. J. Dwayne Miller and members of his research group for their insightful discussions on UED experiments. This work was supported by the Natural Sciences and Engineering Research Council of Canada. E.Ya. Sherman acknowledges support of the Ikerbasque foundation and the University of the Basque Country, grant GIU07/40.

## APPENDIX A: MATHEMATICAL DETAILS FOR EQUATION (41)

We move from Eq. (40) and (41) by a change in variables. We first introduce vectors in the $\hat{\mathbf{m}}$ and $\hat{\mathbf{l}}$ directions, $\mathbf{p}_m \equiv p_m \hat{\mathbf{m}}$ and $\mathbf{p}_l \equiv p_l \hat{\mathbf{l}}$. This allows us to write

$$\int d\hat{\mathbf{m}} d\hat{\mathbf{l}} = \frac{1}{p^4} \int d\mathbf{p}_m d\mathbf{p}_l \delta(p_m - p)\delta(p_l - p_m).$$

We then apply the following change in coordinates:

$$\tilde{\mathbf{p}} = (\mathbf{p}_m + \mathbf{p}_l)/2,$$

$$\mathbf{q} = \mathbf{p}_l - \mathbf{p}_m.$$

Letting $\mathbf{q} = \mathbf{s} + \nu\tilde{\mathbf{p}}/|\tilde{\mathbf{p}}|$, the $\delta$ functions become

$$\delta(p_l - p_m) = \frac{\sqrt{\tilde{p}^2 + s^2/4}}{\tilde{p}} \delta(\nu) \tag{A1}$$

$$\delta(p_m - p) = \delta(p - \sqrt{\tilde{p}^2 - \tilde{p}\nu + \nu^2/4 + s^2/4})$$

$$= \frac{p}{\sqrt{p^2 - s^2/4}} \delta[\tilde{p} - p(s)], \tag{A2}$$

where Eq. (A2) results from the integration over $\nu$, and $p(s) = \sqrt{p^2 - s^2/4}$.

Equation (40) is rewritten as (with $d\mathbf{q} = d^2 s d\nu$)

$$\mathcal{F}(p\hat{\mathbf{n}}_1, p\hat{\mathbf{n}}_2) = \sum_{j,k} \frac{1}{p^4} \int d^3u d^3\tilde{p} d^2 s d\nu \frac{\sqrt{\tilde{p}^2 + s^2/4}}{\tilde{p}} \delta(\nu) \frac{p\delta(\tilde{p} - p(s))}{\sqrt{p^2 - s^2/4}} W(\mathbf{u}, \tilde{\mathbf{p}}) e^{i\mathbf{u}\cdot\mathbf{q}/\hbar} e^{i\mathbf{\Lambda}_{jk}\cdot(p\hat{\mathbf{n}}_1 - p\hat{\mathbf{n}}_2)/\hbar} e^{-i\mathbf{R}_{jk}\cdot(p\hat{\mathbf{n}}_1 + p\hat{\mathbf{n}}_2)/2\hbar}$$
$$\times e^{i\mathbf{R}_{jk}\cdot\tilde{\mathbf{p}}/\hbar} e^{-i\mathbf{\Lambda}_{jk}\cdot\mathbf{q}/\hbar} f_j\left(p\hat{\mathbf{n}}_2 \leftarrow \tilde{\mathbf{p}} - \frac{1}{2}\mathbf{q}\right) f_k^*\left(p\hat{\mathbf{n}}_1 \leftarrow \tilde{\mathbf{p}} + \frac{1}{2}\mathbf{q}\right), \tag{A3}$$

where $\mathbf{\Lambda}_{jk} = (\mathbf{R}_j + \mathbf{R}_k)/2$ and $\mathbf{R}_{jk} = \mathbf{R}_j - \mathbf{R}_k$. Integrating over $\nu$ sets $\nu = 0$ and $\mathbf{q} = \mathbf{s}$ everywhere in the above expression, and integrating over the magnitude of $\tilde{\mathbf{p}}$ evaluates the remaining $\delta$ function. Finally, renaming $\tilde{\mathbf{p}}/|\tilde{\mathbf{p}}|$ to $\hat{\mathbf{p}}$, we arrive at Eq. (41).

## APPENDIX B: SIMPLIFICATION OF FRESNEL TERMS

This section details the simplification from Eq. (45)–(49). The far-field approximation (34) applied to Eq. (45) leads to phases of form (36). We then expand $|\mathbf{r} - \mathbf{R}_j|$ for small $R_j/r$,

$$|\mathbf{r} - \mathbf{R}_j| = r\sqrt{1 + R_j^2/r^2 - 2\mathbf{R}_j \cdot \hat{\mathbf{r}}/\mathbf{r}}$$
$$\approx r[1 - R_j \hat{\mathbf{R}}_j \cdot \hat{\mathbf{r}}/r + R_j^2(1 - (\hat{\mathbf{R}}_j \cdot \hat{\mathbf{r}})^2)/2r^2$$
$$+ R_j^3 \hat{\mathbf{R}}_j \cdot \hat{\mathbf{r}}(1 - (\hat{\mathbf{R}}_j \cdot \hat{\mathbf{r}})^2)/2r^3 + \cdots] \tag{B1}$$

and similarly expand $|\mathbf{r} - \mathbf{R}_k|$ for small $R_k/r$. We present the expansion of the phase factors as

$$\frac{p}{\hbar}(|\mathbf{r} - \mathbf{R}_j| - |\mathbf{r} - \mathbf{R}_k|) = -(\mathbf{R}_j - \mathbf{R}_k) \cdot \hat{\mathbf{r}} p/\hbar$$
$$+ \frac{p}{\hbar} \sum_n g_n(\mathbf{R}_j, \mathbf{R}_k, \hat{\mathbf{r}})/r^n. \tag{B2}$$

From Eq. (B1), the combination of the expansions gives the first correction term $g_1$,

$$g_1(\mathbf{R}_j, \mathbf{R}_k, \hat{\mathbf{r}}) = R_j^2 - R_k^2 - (\mathbf{R}_j \cdot \hat{\mathbf{r}})^2 + (\mathbf{R}_k \cdot \hat{\mathbf{r}})^2$$
$$= 2\Lambda_{jk} \cdot \mathbf{R}_{jk} - \left(\mathbf{\Lambda}_{jk} \cdot \hat{\mathbf{r}} + \frac{1}{2}\mathbf{R}_{jk} \cdot \hat{\mathbf{r}}\right)^2$$
$$+ \left(\mathbf{\Lambda}_{jk} \cdot \hat{\mathbf{r}} - \frac{1}{2}\mathbf{R}_{jk} \cdot \hat{\mathbf{r}}\right)^2$$
$$= 2\mathbf{\Lambda}_{jk} \cdot \mathbf{R}_{jk} - 2(\mathbf{\Lambda}_{jk} \cdot \hat{\mathbf{r}})(\mathbf{R}_{jk} \cdot \hat{\mathbf{r}})$$
$$= 2\Lambda_{jk} R_{jk}[\hat{\mathbf{\Lambda}}_{jk} \cdot \hat{\mathbf{R}}_{jk} - \hat{\mathbf{R}}_{jk} \cdot \hat{\mathbf{r}} \cos\beta], \tag{B3}$$

where $\mathbf{\Lambda}_{jk} = (\mathbf{R}_j + \mathbf{R}_k)/2$, $\mathbf{R}_{jk} = \mathbf{R}_j - \mathbf{R}_k$, and $\beta$ is the angle between $\mathbf{\Lambda}_{jk}$ and $\hat{\mathbf{r}}$ as denoted in Fig. 16. For large $\Lambda_{jk}$, we can approximate $\pi/2 - \beta \lesssim \vartheta_B$. Since $\vartheta_B \approx 10^{-2}$, we expand the last line of Eq. (B3) for small $\vartheta_B$, which yields $\hat{\mathbf{\Lambda}}_{jk} \cdot \hat{\mathbf{R}}_{jk} - \hat{\mathbf{R}}_{jk} \cdot \hat{\mathbf{r}} \cos\beta \approx \hat{\mathbf{\Lambda}}_{jk} \cdot \hat{\mathbf{R}}_{jk} - \vartheta_B \hat{\mathbf{R}}_{jk} \cdot \hat{\mathbf{r}}$. The maximum value of $\mathbf{\Lambda}_{jk} \cdot \mathbf{R}_{jk}$ is much larger than the maximum possible value of $\vartheta_B \Lambda_{jk} \mathbf{R}_{jk} \cdot \hat{\mathbf{r}}$, for possible atom pairs $(j,k)$. Hence, to neglect the first correction term we require that

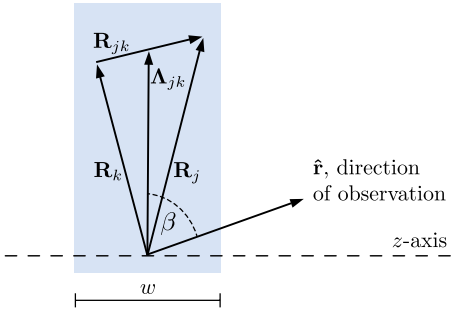


FIG. 16. (Color online) Thin film geometry used in the expansion of the phase factors.

$$\frac{p}{\hbar r} g_1(\mathbf{R}_j, \mathbf{R}_k, \hat{\mathbf{r}}) \lesssim \max\left[\frac{p}{\hbar r} \mathbf{\Lambda}_{jk} \cdot \mathbf{R}_{jk}\right] \ll 1.$$

For large values of $\Lambda_{jk}$, the thin film geometry leads to $\Lambda_{jk} \approx \Lambda_{jk}^T$. From the analysis in Sec. IV B we know the restriction on $\mathbf{\Lambda}_{jk}$ is $\Delta u_T$ from Eq. (46), and the restrictions on $\mathbf{R}_{jk}$ are $L_{T,z}$ from Eq. (47). For large $\Lambda_{jk}$, the unit vector $\hat{\mathbf{\Lambda}}_{jk}$ is approximately in the transverse direction and $\mathbf{R}_{jk} \cdot \hat{\mathbf{\Lambda}}_{jk} \approx R_{jk}^T$, which is restricted by $L_T = \hbar / \Delta p_T^{\mathrm{loc}} \approx 20$ Å (Table I). This leads to

$$\Lambda_{jk} \ll \frac{\hbar r}{p L_T} \approx 10^2 \ \mu\mathrm{m}, \tag{B4}$$

where $r \approx 20$ cm and $p/\hbar \approx 10^2/\text{Å}$ for a typical UED setup. The condition (B4) is not satisfied for the typical UED experimental parameters since the typical electron bunch extends over a spot size of around 100 $\mu$m. The first correction term (A6) must be kept.

We now turn to the second $n=2$ correction in Eq. (B2). In terms of $\mathbf{\Lambda}_{jk}$ and $\mathbf{R}_{jk}$, for $\Lambda_{jk} \gg R_{jk}$ the function $g_2$ in the expansion is

$$\begin{aligned} g_2(\mathbf{R}_j, \mathbf{R}_k, \hat{\mathbf{r}}) &\approx (\mathbf{R}_{jk} \cdot \hat{\mathbf{r}})[\Lambda_{jk}^2 - 3(\mathbf{\Lambda}_{jk} \cdot \hat{\mathbf{r}})^2] + 2(\mathbf{\Lambda}_{jk} \cdot \hat{\mathbf{r}}) \\ &\quad \times (\mathbf{\Lambda}_{jk} \cdot \mathbf{R}_{jk}) \\ &= \Lambda_{jk}^2 R_{jk} [\hat{\mathbf{R}}_{jk} \cdot \hat{\mathbf{r}} - 3\hat{\mathbf{R}}_{jk} \cdot \hat{\mathbf{r}} \cos^2 \beta \\ &\quad + 2\hat{\mathbf{R}}_{jk} \cdot \hat{\mathbf{\Lambda}}_{jk} \cos \beta] \\ &\approx \Lambda_{jk}^2 R_{jk} [\hat{\mathbf{R}}_{jk} \cdot \hat{\mathbf{r}} + 2\vartheta_B \hat{\mathbf{R}}_{jk} \cdot \hat{\mathbf{\Lambda}}_{jk} \\ &\quad - 3\vartheta_B^2 \hat{\mathbf{R}}_{jk} \cdot \hat{\mathbf{r}}], \end{aligned} \tag{B5}$$

where again $\pi/2 - \beta \lesssim \vartheta_B$ and we expanded for small $\vartheta_B$. As before, we can neglect the terms involving $\vartheta_B$ and the requirement to neglect the second correction term is

$$\frac{p}{\hbar r^2} g_2(\mathbf{R}_j, \mathbf{R}_k, \hat{\mathbf{r}}) \approx \max[\Lambda_{jk}^2 \mathbf{R}_{jk} \cdot \hat{\mathbf{r}}] \ll 1.$$

Since $\hat{\mathbf{r}}$ is close to the $z$ direction, $\mathbf{R}_{jk} \cdot \hat{\mathbf{r}} \approx \mathbf{R}_{jk}^z \lesssim w$, where $w$ is the width of the film. This leads to

$$\Lambda_{jk} \ll r \sqrt{\frac{\hbar}{pw}}. \tag{B6}$$

For a pair of atoms $(j,k)$, in the transverse direction $\Lambda_{jk}$ is limited as $\Lambda_{jk}^T \lesssim \Delta u_T$ (Eq. (46)) while in the longitudinal direction $\Lambda_{jk}^z$ is limited by the width of the film $w$. Recall inequality (42f),

$$\max[\Delta u_T, w] \ll r \sqrt{\frac{\lambda}{w}}.$$

Hence, if Eq. (42f) is satisfied, so is condition (B6) and the second correction term can be neglected.

For a typical UED experiment with a detection distance $r \approx 10$ cm, $\lambda \approx 0.1$ Å, and a film thickness of $w \approx 50$ nm, inequality (42f) is satisfied since $\max[\Delta u_T, w] = \Delta u_T \approx 10^2$ $\mu$m $\ll r\sqrt{\lambda/w} \approx 10^3$ $\mu$m. In addition, for $\Lambda_{jk} \approx 10^3$ $\mu$m, the ratio $\Lambda_{jk}/r$ becomes of the order $10^{-2}$, which is close to the Born angle $\vartheta_B$, and therefore the angular dependence of the atomic scattering amplitude would become important in the Bragg spot formation.

## APPENDIX C: SIMPLIFICATION OF THE GAUSSIAN $\Gamma_{\mathrm{DIFF}}$ EXPRESSION

We detail the steps taken in arriving at expressions (53) from (49), taking the Wigner function $W(\mathbf{u}, \mathbf{p})$ of the Gaussian form (51). We also discuss how we arrive at Eq. (56) from (53).

Substituting form (51) of $W(\mathbf{u}, \mathbf{p})$ into Eq. (49), we can immediately evaluate the $\delta$ function. We are then left with a Gaussian integral over a single spatial variable in the direction of $\hat{\mathbf{p}}$ that is easily evaluated after changing to the new coordinate system (52). Expanding the exponent terms of the result for small $\theta$, we obtain the terms related to the transverse direction,

$$\begin{aligned} &\theta^2 \left( -\frac{p^2}{2(\Delta p_T^{\mathrm{loc}})^2} + \frac{\Lambda_1^2}{2\Delta u_T^2} + \frac{\Lambda_1^2 (\Delta p_T^{\mathrm{dist}})^2}{2(\Delta p_T^{\mathrm{loc}})^2 \Delta u_T^2} \right) \\ &\quad + \theta \left( \frac{p \Lambda_1 \Delta p_T^{\mathrm{dist}}}{(\Delta p_T^{\mathrm{loc}})^2 \Delta u_T} \right) - \frac{\Lambda_1^2 + \Lambda_2^2}{2\Delta u_T^2} - \frac{(\Lambda_1^2 + \Lambda_2^2)(\Delta p_T^{\mathrm{dist}})^2}{2(\Delta p_T^{\mathrm{loc}})^2 \Delta u_T^2} \\ &= -\frac{(p\theta - \Lambda_1 \Delta p_T^{\mathrm{dist}}/\Delta u_T)^2}{2(\Delta p_T^{\mathrm{loc}})^2} - \frac{\Lambda_2^2 (\Delta p_T^{\mathrm{dist}})^2}{2(\Delta p_T^{\mathrm{loc}})^2 \Delta u_T^2} - \frac{\Lambda_1^2 + \Lambda_2^2}{2\Delta u_T^2} \\ &\quad + \theta^2 \frac{\Lambda_1^2 (\Delta p_T)^2}{2(\Delta p_T^{\mathrm{loc}})^2 \Delta u_T^2}, \end{aligned} \tag{C1}$$

where $\Lambda_{1,2} \equiv \mathbf{\Lambda}_{jk} \cdot \hat{\mathbf{e}}_{1,2}$ and we used Eq. (12) to move to the second line of Eq. (C1).

Recall that for typical UED electron bunches $p \gg \Delta p_T$ [relation (42g) and Table I]. Looking at the $\theta^2$ terms we see that $\Lambda_1^2 \Delta p_T^2 / \Delta u_T^2 \ll p^2$, which lets us neglect the last term of Eq. (C1), and we can write

$$-\frac{(p\theta - \chi_T \Lambda_1)^2}{2(\Delta p_T^{\mathrm{loc}})^2} - \frac{\chi_T^2 \Lambda_2^2}{2(\Delta p_T^{\mathrm{loc}})^2} - \frac{\Lambda_1^2 + \Lambda_2^2}{2\Delta u_T^2}, \tag{C2}$$

where $\chi_T$ is defined in Eq. (51).

The $z$ related terms of the same small $\theta$ expansion of the exponent are more algebraically involved. If one again makes approximations valid for typical UED bunches, $\Delta p_z \approx \Delta p_z^{\mathrm{dist}} \gg \Delta p_z^{\mathrm{loc}}$ and $\Delta u \approx \Delta u_z$, the simplifications leads to

$$\exp[-(p - p_0 - \theta \Lambda_1 \Delta p_z^{\mathrm{dist}}/\Delta u_z)^2/(\Delta p_z^{\mathrm{loc}})^2], \tag{C3}$$

where $\theta\Lambda_1$ is the $z$ component of the projection $\Lambda_{jk} \cdot \hat{\mathbf{e}}_1 = \Lambda_1$. Expression (C3) corresponds to the term $\exp[-(p_z - p_0 - \chi_z z)^2/(2(\Delta p_z^{\mathrm{loc}})^2)]$ in the Wigner function. Expanding the exponential we get

$$\frac{(p - p_0)^2}{(\Delta p_z^{\mathrm{loc}})^2} - \frac{2(p - p_0)\chi_z \theta \Lambda_1}{(\Delta p_z^{\mathrm{loc}})^2} + \frac{(\chi_z \theta \Lambda_1)^2}{(\Delta p_z^{\mathrm{loc}})^2}.$$

The first term shows that $p$ is very close to the average bunch momentum $p_0$. For a thin film of thickness $w$, one has $\theta\Lambda_1 \lesssim w$. Given an order of magnitude value of $w \approx 50$ nm for a thin film, and typical UED bunch parameters, we estimate that $\chi_z \theta \Lambda_1 \approx 5 \times 10^{-2}/\mu\mathrm{m} \ll \Delta p_z^{\mathrm{loc}}$. Hence we only include the term $\exp[-(p - p_0)^2/(\Delta p_z^{\mathrm{loc}})^2]$ and Eq. (C2) in Eq. (53).

To move from Eq. (53)–(56), we rewrite Eq. (C2) as

$$-\frac{(\mathbf{p}_\perp - \chi_T \mathbf{R})^2}{2(\Delta p_T^{\mathrm{loc}})^2} - \frac{R^2}{2\Delta u_T^2},$$

where $\mathbf{p}_\perp = (p_x, p_y)$, and $\mathbf{R} \equiv (\mathbf{\Lambda}_{jk} \cdot \hat{\mathbf{e}}_1)\hat{\mathbf{e}}_1 + (\mathbf{\Lambda}_{jk} \cdot \hat{\mathbf{e}}_2)\hat{\mathbf{e}}_2$ and hence $R^2 \equiv \Lambda_1^2 + \Lambda_2^2$. We use the following algebraic identity. Given two vectors $\mathbf{a}$ and $\mathbf{b}$, if $\mathbf{b} = \mathbf{b}_\parallel + \mathbf{b}_\perp$, where $\mathbf{b}_\perp$ is perpendicular to the $\hat{\mathbf{a}}$ direction, then $\mathbf{a} \cdot \mathbf{b}_\perp = \mathbf{b}_\parallel \cdot \mathbf{b}_\perp = 0$ and

$$(\mathbf{a} - \mathbf{b})^2 = ((\mathbf{a} - \mathbf{b}_\parallel) - \mathbf{b}_\perp)^2 = (\mathbf{a} - \mathbf{b}_\parallel)^2 + \mathbf{b}_\perp^2.$$

The vector $\mathbf{p}_\perp$ is perpendicular to $\hat{\boldsymbol{z}}$, as is the component $(\mathbf{\Lambda}_{jk} \cdot \hat{\mathbf{e}}_2)\hat{\mathbf{e}}_2$. This is how we arrive at Eq. (56).


[1] B. J. Siwick, J. R. Dwyer, R. E. Jordan, and R. J. D. Miller, Science **302**, 1382 (2003).
[2] R. J. D. Miller, J. R. Dwyer, C. T. Hebeisen, R. E. Jordan, and B. J. Siwick, Proc. SPIE **5448**, 485 (2004).
[3] B. J. Siwick, J. R. Dwyer, R. E. Jordan, and R. D. Miller, Chem. Phys. **299**, 285 (2004).
[4] M. Harb, R. Ernstorfer, T. Dartigalongue, C. T. Hebeisen, R. E. Jordan, and R. J. D. Miller, J. Phys. Chem. B **110**, 25308 (2006).
[5] J. R. Dwyer, R. E. Jordan, C. T. Hebeisen, M. Harb, R. Ernstorfer, T. Dartigalongue, and R. J. D. Miller, J. Mod. Opt. **54**, 905 (2007).
[6] J. Williamson, M. Dantus, S. Kim, and A. Zewail, Chem. Phys. Lett. **196**, 529 (1992).
[7] H. Ihee, V. A. Lobastov, U. M. Gomez, B. M. Goodson, R. Srinivasan, C.-Y. Ruan, and A. H. Zewail, Science **291**, 458 (2001).
[8] S. Ryu, R. M. Stratt, K. K. Baeck, and P. M. Weber, J. Phys. Chem. A **108**, 1189 (2004).
[9] J. S. Baskin and A. H. Zewail, ChemPhysChem **6**, 2261 (2005).
[10] J. S. Feenstra, S. T. Park, and A. H. Zewail, J. Chem. Phys. **123**, 221104 (2005).
[11] Y. He, A. Gahlmann, J. S. Feenstra, S. T. Park, and A. H. Zewail, Chem. Asian J. **1**, 56 (2006).
[12] S. T. Park, J. S. Feenstra, and A. H. Zewail, J. Chem. Phys. **124**, 174707 (2006).
[13] D.-S. Yang, N. Gedik, and A. H. Zewail, J. Phys. Chem. C **111**, 4889 (2007).
[14] A. Janzen, B. Krenzer, P. Zhou, D. von der Linde, and M. Horn-von Hoegen, Surf. Sci. **600**, 4094 (2006).
[15] M. T. Seidel, S. Chen, and A. H. Zewail, J. Phys. Chem. C **111**, 4920 (2007).
[16] C.-Y. Ruan, Y. Murooka, R. K. Raman, and R. A. Murdick, Nano Lett. **7**, 1290 (2007).
[17] A. M. Michalik and J. E. Sipe, J. Appl. Phys. **99**, 054908 (2006); **103**, 129901 (2008).
[18] R. L. Liboff, *Kinetic Theory: Classical, Quantum and Relativistic Descriptions*, 3rd ed. (Springer, New York, 1998).
[19] J. R. Taylor, *Scattering Theory* (Wiley, New York, 1972).
[20] W. E. King, G. H. Campbell, A. Frank, B. Reed, J. F. Schmerge, B. J. Siwick, B. C. Stuart, and P. M. Weber, J. Appl. Phys. **97**, 111101 (2005).
[21] J. R. Dwyer, R. E. Jordan, C. T. Hebeisen, M. Harb, R. Ernstorfer, T. Dartigalongue, and R. J. D. Miller, J. Mod. Opt. **54**, 923 (2007).
[22] N. Bleistein and R. A. Handelsman, *Asymptotic Expansions of Integrals* (Dover, New York, 1986).
[23] G. R. Fowles, *Introduction to Modern Optics*, 2nd ed. (Holt, Rinehart, and Winston, New York, 1968).
[24] L. D. Landau and E. M. Lifshits, *Quantum Mechanics : Non-Relativistic Theory*, 3rd ed. (Pergamon, New York, 1977).
[25] P. D. McCaffrey, J. K. Dewhurst, D. W. H. Rankin, R. J. Mawhorter, and S. Sharma, J. Chem. Phys. **128**, 204304 (2008).